Contribution of TRPC channels in human and experimental pulmonary arterial hypertension

Bastien Masson, Anais Saint-Martin Willer, Mary Dutheil, Lucille Penalva, Hélène Le Ribeuz, Kristelle El Jekmek, Yann Ruchon, Sylvia Cohen-Kaminsky, Jessica Sabourin, Marc Humbert, et al.

Contribution of TRPC channels in human and experimental pulmonary arterial hypertension

Short title: TRPC channels in PAH

Bastien Masson[1,2], Anais Saint-Martin Willer[1,2], Mary Dutheil[1,2,3], Lucille Penalva[1,2], Hélène Le Ribeuz[1,2], Kristelle El Jekmek[1,2], Yann Ruchon[1,2,3], Sylvia Cohen-Kaminsky[1,2], Jessica Sabourin[4], Marc Humbert[1,2,5], Olaf Mercier[1,2,6], David Montani[1,2,5], Véronique Capuano[1,2,3] and Fabrice Antigny[1,2]

[1]Université Paris-Saclay, Faculté de Médecine, Le Kremlin-Bicêtre, France. (B.M, H.L-R, M.D, L.P, A. SM-W, Y. R,C.E-J, S.C-K, M.H, D.M, V.C and F.A)

[2]INSERM UMR_S 999 « Hypertension pulmonaire : Physiopathologie et Innovation Thérapeutique », Hôpital Marie Lannelongue, Le Plessis-Robinson, France. (B.M, H.L-R, M.D, L.P, A. SM-W, Y. R, C.E-J, S.C-K M.H, D.M, V.C and F.A)

[3]Hôptal Marie Lannelongue, Groupe Hospitalier Paris Saint-Joseph, Le Plessis Robinson, France. (Y.R, M.D, V.C)

[4]Inserm, UMR-S 1180, Signalisation et Physiopathologie Cardiovasculaire, Université Paris-Saclay, Châtenay-Malabry, France. (J.S)

[5]Assistance Publique - Hôpitaux de Paris (AP-HP), Service de Pneumologie et Soins Intensifs Respiratoires, Centre de Référence de l'Hypertension Pulmonaire, Hôpital Bicêtre, Le Kremlin-Bicêtre, France. (M.H, D.M)

[6]Service de Chirurgie Thoracique, Vasculaire et Transplantation Cardio-Pulmonaire, Hôpital Marie Lannelongue, Groupe Hospitalier Paris Saint Joseph, Le Plessis Robinson, France. (O.M)

Corresponding author: Fabrice Antigny, INSERM UMR_S 999, Hôpital Marie Lannelongue, 133, Avenue de la Résistance, F-92350 Le Plessis Robinson, France.

Tel. : (33) 1 40 94 22 99; E-mail: fabrice.antigny@inserm.fr

ABSTRACT

Pulmonary arterial hypertension (PAH) is due to progressive distal pulmonary artery (PA) obstruction leading to right ventricular hypertrophy and failure. Exacerbated store-operated Ca^{2+} entry (SOCE) contributes to PAH pathogenesis, mediating human PA smooth muscle cells (hPASMCs) abnormalities. The transient receptor potential canonical channels (TRPC family) are Ca^{2+}-permeable channels contributing to SOCE in different cell types, including PASMCs. However, the properties, signaling pathways, and contribution to Ca^{2+} signaling of each TRPC isoform are unclear in human PAH.

We studied *in vitro* the impact of TRPC knockdown on control and PAH-hPASMCs function. *In vivo*, we analyzed the consequences of pharmacological TRPC inhibition using the experimental model of pulmonary hypertension (PH) induced by monocrotaline (MCT)-exposure.

Compared to control-hPASMCs cells, in PAH-hPASMCs, we found a decreased TRPC4 expression, overexpression of TRPC3 and TRPC6, and unchanged TRPC1 expression. Using the siRNA strategy, we found that the knockdown of TRPC1-C3-C4-C6 reduced the SOCE and the proliferation rate of PAH-hPASMCs. Only TRPC1 knockdown decreased the migration capacity of PAH-hPASMCs. After PAH-hPASMCs exposure to the apoptosis inducer staurosporine, TRPC1-C3-C4-C6 knockdown increased the percentage of apoptotic cells, suggesting that these channels promote apoptosis resistance. Only TRPC3 function contributed to exacerbated calcineurin activity. In the MCT-PH rats' model, only TRPC3 protein expression was increased in lungs compared to control rats, and *in vivo* "curative" administration of a TRPC3 inhibitor attenuated PH development in rats.

These results suggest that TRPC channels contribute to PAH-hPASMCs dysfunctions, including SOCE, proliferation, migration, apoptosis resistance, and could be considered as therapeutic targets in PAH.

Keywords: TRPC, PAH, calcineurin, Pyr3, apoptosis, proliferation, migration, contraction

New and Noteworthy

TRPC3 is increased in human and experimental pulmonary arterial hypertension (PAH).

In PAH pulmonary arterial smooth muscle cells, TRPC3 participates in the aberrant store-operated Ca2+ entry contributing to their pathological cell phenotypes (exacerbated proliferation, enhanced migration, apoptosis resistance, and vasoconstriction).

Pharmacological in vivo inhibition of TRPC3 reduces the development of experimental PAH.

Even if other TRPC acts on PAH development, our results prove that TRPC3 inhibition could be considered as an innovative treatment for PAH.

GRAPHICAL ABSTRACT

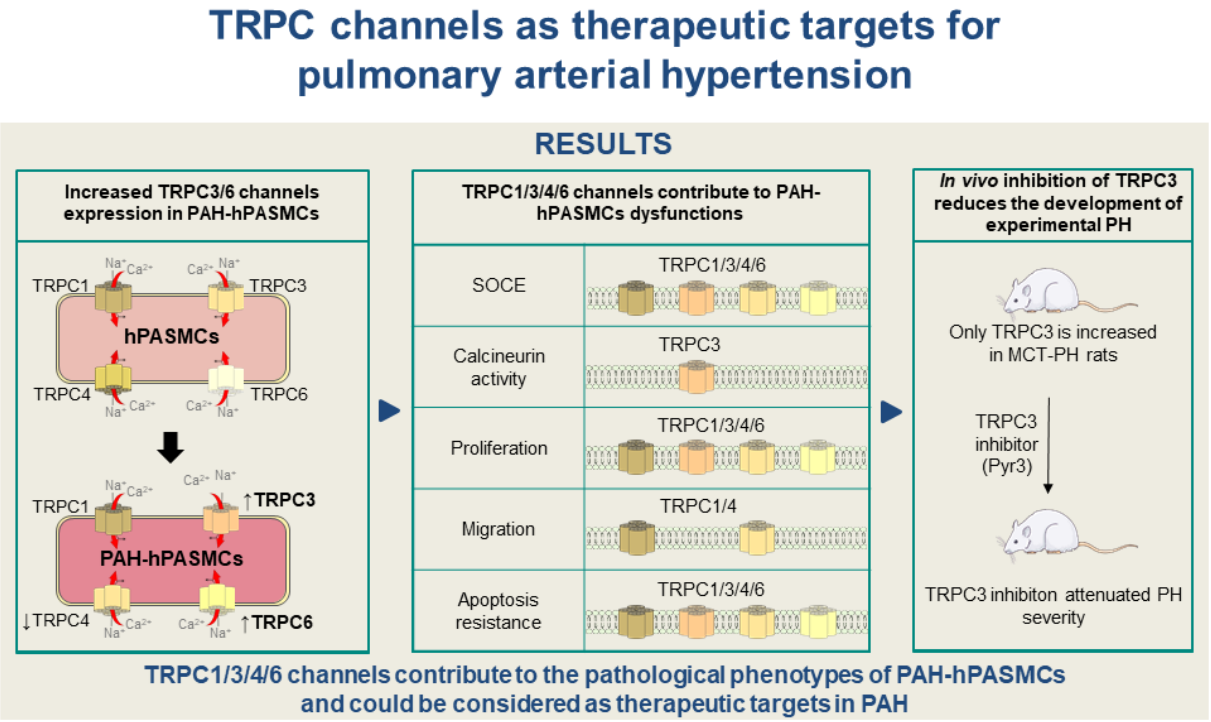

INTRODUCTION

Pulmonary arterial hypertension (PAH) is a rare and progressive cardiovascular disease resulting from obstruction of the distal pulmonary artery (PA), leading to elevated pulmonary vascular resistance (PVR), right ventricular (RV) hypertrophy, and ultimately RV failure (RVF) and death[1]. According to the new guidelines, PAH is defined by a mean PA pressure >20 mmHg, a PVR >2 Wood units, and a PA wedge pressure ≤15 mmHg at rest[2]. PAH is a multifactorial syndrome that can be explained by dysfunction of all cell types composing the pulmonary circulation, particularly PA smooth muscle cells (PASMC), including vasoconstriction, excessive migration, apoptosis resistance, and hyperproliferation[1]. Despite adequate therapeutics that prolong patient survival, lung transplantation is the ultimate therapy for eligible PAH patients, meaning that identifying novel targets is needed to improve patient management.

We demonstrated that exacerbated intracellular calcium concentration ($[Ca^{2+}]i$) contributes to PASMC dysfunction in PAH[3]. Among Ca^{2+} channel families, store-operated Ca^{2+} channels (SOC) may play a critical role in regulating PASMC function[3,4]. Three essential components constitute SOCs: the endoplasmic/sarcoplasmic reticulum (ER/SR) Ca^{2+} sensor belonging to the stromal interaction molecule family (STIM1-2) and two Ca^{2+} channels, namely TRPC (Transient Receptor Potential Canonical) and Orai (Orai1-3)[3]. TRPC channels are non-selectively permeable to cations, including potassium (K^+), sodium (Na^+), calcium (Ca^{2+}), and magnesium (Mg^{2+})[5]. The TRPC subfamily consists of seven members, from TRPC1 to TRPC7, and TRPC2 is a pseudogene in humans[6]. TRPC contributes to the proliferation and migration of systemic vascular endothelial cells and smooth muscle cells[7]. Gene polymorphism in the *TRPC6* gene was identified in a few PAH patients, predisposing them to develop PAH[8]. The double *trpc1/trpc6* knockout mice are protected from chronic hypoxia (CH)-induced PH[9]. The triple *trpc1/trpc3/trpc6* knockout mice have decreased hypoxic pulmonary vasoconstriction without any consequence on pulmonary vascular obstruction induced by CH exposure[10]. However, in human PASMCs (hPASMCs), the role of each expressed TRPC channel in PAH pathological phenotypes remains elusive.

In the present study, we investigated the expression and function of TRPC isoforms in human PA and human PASMCs isolated from control (control-hPASMCs) and PAH patients (PAH-hPASMCs) and their contribution to PAH-hPASMC phenotypes (proliferation, migration, contraction, apoptosis

resistance). We also evaluated *in vivo* the contribution of TRPC3 to the development of experimental PH caused by monocrotaline (MCT)-exposure in rats. Overall, we show that all expressed TRPC channels contribute to cellular dysfunction occurring in PAH-hPASMCs and that targeting TRPC could constitute an innovative therapeutic approach in PAH.

MATERIALS AND METHODS

Chemicals

MCT, staurosporine, endothelin-1, histamine, PDTC, cytosine arabinoside, and nifedipine were obtained from Sigma-Aldrich. MCV1 (Calbiochem) and U46619 were obtained from R&D Systems. Fura-2-AM was obtained from Thermo Fisher Scientific. KB-R7943 and Pyr3 were obtained from TOCRIS. LW6 was obtained from CliniSciences.

Human lung specimens

Human lung specimens were obtained from lung transplantation in 12 patients with PAH and from lobectomy or pneumonectomy for localized lung cancer from 10 patients as control subjects. Female PAH patients represent 70% of primary cells. PAs (diameter:3–5 mm) were isolated from non-tumoral areas in the lung specimens of control subjects. Transthoracic echocardiography was performed preoperatively in control subjects to rule out PH. Patients with PAH underwent genetic counseling and were provided written informed consent for genetic analysis. The demographic information of PAH and control patients are presented in **Supplemental Table 1**.

Patients were part of the French Network on Pulmonary Hypertension, a program approved by our institutional ethics committee, and provided written informed consent (Protocol N8CO-08- 003, ID RCB: 2008-A00485-50, approved on June 18th, 2008). Patients studied were part of a program approved by our institutional Ethics Committee and had given written informed consent (ID RCB: 2018-A01252-53, approved on June 18, 2006). All human tissues were obtained with written informed consent from transplant recipients or families of organ donors following the Declaration of Helsinki.

Human PASMC culture from PAH and control patients

hPASMCs were isolated from pulmonary arteries (diameter:3–5 mm) obtained during lung transplantation for PAH patients and lobectomy or pneumonectomy of localized lung cancer from control subjects. Pulmonary arteries were excised at a distance from tumor areas.

PAs (diameter:3–5 mm) were kept in DMEM at 4°C before their intimal cell layer and residual adventitial tissue were stripped of fusing forceps. The dissected media of the vessels was then cut into small pieces (3–5 mm), which were transferred into 6 well plates (one piece per well). The explants adhered to the support, and to allow the PASMCs to grow out, the explants were incubated in DMEM supplemented with 20 % fetal bovine serum, 2 mM L-glutamine, and antibiotics (100 U/ml penicillin and 0.1 mg/ml streptomycin,10 U/ml Epidermal Growth Factor, insulin). After 2 weeks of incubation, the hPASMCs collected in the culture medium and the vessel tissues were transferred into new cell-culture flasks. Cultured hPASMCs were used between passages 3 and 5[11,12].

Characterization of cultured control and PAH-hPASMCs was assessed by positive staining with antibodies against smooth muscle cell α-actin, desmin, and vinculin[13].

Animal models

The facility is licensed by the French Ministry of Agriculture (agreement N° C92-019-01). This study was approved by the Committee on the Ethics of Animal Experiments (CEEA26 CAP Sud). Animal experiments were performed following the guidelines of Directive 2010/63/EU on September 22nd, 2010, of the European Parliament on the protection of animals used for scientific purposes and complied with the French institution's animal care and handling guidelines.

In-vivo experiments were performed according to clinical trial standards. Rats were randomly distributed between groups, and all methods and analyses were performed with researchers blinded to the conditions. All rats received a number known only by the experimenter who delivered the treatment. Before sacrifice (day 21), all rats underwent an evaluation by closed-chest right heart catheterization. This experiment was performed by a blinded experimenter who did not know the correspondence between rat number and treatment. Hemodynamic parameters were analysed in a blinded fashion.

PH was induced by a single MCT injection (60 mg/kg, s.c.) in male Wistar rats (4 weeks old). MCT was dissolved in 1 N HCl and neutralized with 1 N NaOH. Control animals received the same volume of saline solution. Pyr3 was dissolved in DMSO. MCT-exposed Wistar rats were treated with Pyr3(1

mg/kg/day in DMSO, daily i.p. injection) from week 2 (W2) to week 3 (W3). Control animals received the same volume of DMSO.

Hemodynamic measurements and tissue collection

Rats were placed under general anesthesia and spontaneous breathing with an isoflurane Rodent Anesthesia System (Minerve Esternay, France) (maintenance: isoflurane 2 % in room air). Hemodynamics parameters, such as heart rate (HR), right ventricular (RV) systolic pressure (RVSP; mmHg), and cardiac output (CO; mL/min), were blindly measured in unventilated anesthetized rats using a closed-chest technique. Under profound anesthesia (5 % isoflurane), animals were euthanized. After catheterization, tissues were collected, and Fulton's index was calculated as the ratio of RV weight to left ventricular (LV) plus septal (S) weight (RV ÷ LV + S).

siRNA transfection

PASMCs were transfected in suspension by incubating 4×10^5 cells in a solution containing 500 µL of Opti-MEM (Gibco, ref 31985-062), 3 µL of Lipofectamine RNAiMax (Invitrogen, ref 13778-150), and 100 nM of a specific *Silencer*™ Select siRNA against TRPC1 (siTRPC1, #s14411, Thermo Fisher Scientific), or TRPC3 (siTRPC3, #s14413, Thermo Fisher Scientific), or TRPC4 (siTRPC4, #s229618, Thermo Fisher Scientific), or TRPC6 (siTRPC6, #s14421, Thermo Fisher Scientific) as well as a *Silencer*™ Select negative control (siControl) according to the manufacturer's protocol. All experiments were performed 72 h after PAH-hPASMCs transfection.

Isometric tension measurement

Rat intralobar main PAs were mounted on an emkaBATH4 modular tissue bath system (EMKA Technology, Paris, France) coupled with IOX software (EMKA Technologies). As determined in preliminary experiments, rat PAs were set at an optimal length by equilibration against a passive load of 0.3 g. After adding Krebs solution, vessels were contracted with 100 mmol/L K^+-containing solutions (K100). Once a plateau was reached, the vessels were washed with Krebs solution for 30 min. DMSO or Pyr3 (1 µmol/L) was pre-treated before the dose response to U46619 (0.1 nM to 3 µM). The relaxation responses were expressed as the percentage of the pre-contractile response obtained with U46619.

Reverse transcription-quantitative PCR (RT-qPCR)

Total gene expression was quantified using qPCR following the standard protocol for ready-to-use qPCR SignArrays (AnyGenes) on a StepOne Plus Real-Time PCR System (Life Technologies)[15]. Predesigned probe sets used in the experiments were Human TRPC1 NM_001251845.1; Human TRPC3 NM_001130698.2; Human TRPC4 NM_016179.4; Human TRPC6 NM_004621.6; Human Orai1 NM_001277961.3; Human STIM1; Human β-Actin NM_001101.

Pulmonary vessel remodeling analysis

The lungs were fixed in 4 % paraformaldehyde, embedded in paraffin, and serially sectioned (5 µm). A pulmonary pathologist performed the histopathological evaluation of the lungs, blinded to treatment group assignments. The morphometric analyses were performed on sections stained with hematein-eosin-Safran (HES). The lung samples from all rat groups were analyzed by conventional light microscopy using quantitative semiautomated software (NIS-BR; Nikon, Champigny sur Marne, France). Vascular remodeling was assessed in all the pulmonary vessels of size 50 µm to 100 µm identified in 20 randomly selected microscopic fields per tissue section. The wall thickness was calculated using the following equation: (External diameter - Internal diameter) / (External diameter) × 100.

Cardiac histological assessment

Hearts were fixed in 4 % paraformaldehyde, paraffin-embedded, and serially sectioned (5 µm). To assess heart fibrosis, heart sections were stained with Sirius red (0.1 %). Pictures were recorded at 10X on an EVOS microscope (Invitrogen). RV fibrosis was quantified using Image J software.

The level of cardiomyocyte hypertrophy was assessed by analyzing RV sections stained with FITC-conjugated wheat germ agglutinin (WGA) (50 µg/ml) and then observed on an EVOS microscope (Invitrogen). Pictures were recorded at 40X, and RV cardiomyocytes' diameters were determined using Image J software [16].

Intracellular Ca^{2+} measurements

hPASMCs were plated on 18-mm glass coverslips and loaded with 2 µmol/L Fura-2-AM dissolved in DMSO plus 20% pluronic acid (Life Technologies) and then incubated at room temperature for 30 min in darkness in Krebs solution (in mmol/L: 135 NaCl, 5.9 KCl, 2 $CaCl_2$, 1 $MgCl_2$, 10 HEPES, 10 D-glucose) at pH 7.4. Loaded cells were washed twice with the physiological solution before imaging. Ca^{2+} images were obtained using a microscope (Olympus IX71) equipped with a Sutter Fluo Lambda 421 LED system (Sutter Instrument Company, Novato, CA, USA), which rapidly changed the excitation wavelengths between 340 nm and 380 nm. Emission was measured at 510 nm.

The Ca^{2+}-free solution contained 1 mmol/L EGTA instead of 2 mmol/L $CaCl_2$ + nifedipine (L-type Ca^{2+} channel inhibitor) + KB-R7943 (Na^+/Ca^{2+} exchanger inhibitor). Ca^{2+} imaging measurements were performed at room temperature. Due to the high transfection efficiency (90% of transfected cells), cytosolic Ca^{2+} measurements were performed on the whole cell population. Image acquisition in selected cells and analysis was performed with MetaFluor® 7.8 imaging software (Molecular Devices).

Immunoblot analysis

Total protein from human or rat lungs or isolated PA tissue samples or cell samples from rats or humans (diameter:3–5 mm) were prepared in lysis buffer containing 1% Igepal, 20mM Tris HCl, 137 mM NaCl, 10% Glycerol, 2 mM EDTA, 1 mM Na3VO4, leupeptin 10 µg/µl, pepstatin 10 µg/µl, aprotinine 10 µg/µl and protease inhibitor cocktail (aprotinin, leupeptin, and PefaBloc [Roche, Meylan, France]). Protein lysates (40 µg) were separated on SDS-PAGE and transferred to a nitrocellulose membrane[17]. After blocking, membranes were incubated in Tris Buffered Saline + tween and 5 % nonfat milk overnight at 4°C with primary antibodies at adequate concentrations (**Supplemental Table 2**).

Blots were then incubated with horseradish peroxidase (HRP)-conjugated goat anti-mouse diluted 1:10000 (Cell Signaling) or with HRP-conjugated goat anti-rabbit diluted 1:5000 (Cell Signaling), respectively. Antibodies were revealed using Enhanced chemiluminescence reagents (Perkin Elmer). ImageJ Software was used to quantify the level of protein expression. The list of antibodies used is presented in **Supplemental Table 2**. β-Actin was used as a loading control.

Immunofluorescence staining

Paraffin-embedded lung sections (5 µm) were dewaxed in toluene, and antigens were retrieved in Power Universal Antigen Retrieval buffer pH 9,5 (Leica ref PV6125 BR02-1000) for 20 minutes at 95°C. Slices were saturated with human (10 %) and donkey (10 %) sera in phosphate-buffered saline for 1 hour at room temperature.

Free aldehyde groups from Paraformaldehyde fixation were quenched for 10 min with 50 mM NH4Cl solution. Sections were saturated with human (10 %) and goat (10 %) sera in PBS for 1 h at room temperature. Primary and secondary antibodies were used, as reported in Supplemental Table 3. Primary antibodies were detected with secondary antibodies from goat anti-rabbit (1/200). Slides were counterstained with 4',6'-diamidino-2-phenylindole (DAPI)[18]. Mouse IgG and rabbit pre-immune serum (both species of primary antibodies used in this study) were applied to lung sections, followed by anti-rabbit Alexa Fluor 594. Sections were viewed under an LSM 700 microscope (Carl Zeiss, Le Pecq, France) equipped with 405-, 488-, 555-, and 639-nm lasers (Carl Zeiss). Images were recorded and analyzed with ZEN software (Carl Zeiss).

Wound healing assay

We used the wound healing assay to evaluate cell migration. After 48 h of starvation (medium without growth factors: FBS, EGF, and insulin), human PASMCs were plated in a culture insert (Cat. No. 90209; Ibidi) at a density of 1.2×10^4 cells per well in a fresh medium with cytosine arabinoside (10 µmol/L). After allowing cells to attach for 24 h, we removed the culture insert and washed the cells with phosphate-buffered saline to remove non-adherent cells. For siRNA treatment, cells were treated with control siRNA or siRNA against TRPC1 or TRPC3 or TRPC4, or TRPC6 24 h before starvation (72 h before removal of culture inserts). Cell migration into the wound space was quantified using image J. Cell motility/invasion was assessed by the percentage of wound closure 15 h after initiation of wound healing ([(area T0 − area T15) ÷ area T15] × 100).

Calcineurin activity

The activity of PP2A was assessed using the Ser/Thr phosphatase assay system (Cat. No. V2460, Promega). The experiments were performed according to the manufacturer's recommendations. The

optical density values obtained with the molybdate-malachite green-phosphate complex were read at 600 nm with a FlexStation 3 Microplate Reader (Molecular Devices).

PASMCs induced-apoptosis measurement

To induce apoptosis, we treated hPASMCs with staurosporine at 1 µmol/L for 20 min or 50 nmol/L overnight. Cells were washed with cell staining buffer (Cat. No. 420201, BioLegend) and gently detached with trypsin and a cell scraper. After centrifugation (400 *g*, 4°C, 10 min), the supernatant was removed, and cells were stained with the FITC-Annexin V Apoptosis Detection Kit (Cat. No 640914, BioLegend) according to the manufacturer's recommendations. Cells were acquired by flow cytometry (MACSQuant, Miltenyi Biotec), with 75,000 cells counted in each sample and analyzed using Flowlogic software (Inivai Technologies).

PASMCs proliferation measurement

To evaluate cell proliferation, we quantified BrdU incorporation in cells undergoing DNA replication using the DELFIA cell proliferation kit (AD0200, PerkinElmer), according to the manufacturer's recommendations. Different treatments were used, including control siRNA, siRNA against TRPC1 or TRPC3 or TRPC4, or TRPC6. 48h after cell synchronization (0 % SVF) to stimulate cell proliferation, the medium contained 10 % of serum in the presence of 1 µmol/L BrdU for 24 h[14]. The fluorescence signal in the 96-well plate was read with a FlexStation 3 Microplate Reader (Molecular Devices).

Statistical analyses

Analyses were performed using GraphPad Prism software (GraphPad, version 9.0 for Windows) and R statistical computing software. After checking the distribution of our samples with the Shapiro–Wilk Test, differences between the two or more groups were assessed using an unpaired t-test or one-way ANOVA, followed by Tukey's post hoc analysis for multiple comparisons. When conditions of parametric tests were not met, we used either a Mann-Whitney test or Kruskal-Wallis test, followed by Dunn's post hoc analysis for multiple comparisons. All values are reported as mean ± standard error of the mean. Representative images/figures were chosen to represent the mean of each quantification. For all experiments, a *P*-value of <0.05 was considered statistically significant.

RESULTS

Increased TRPC1 and TRPC3 protein expression in pulmonary arteries isolated from PAH patients

We performed immunofluorescent staining in lung sections from control and PAH patients to visualize the localization and expression of TRPC1, TRPC3, TRPC4, and TRPC6 channels. **Figure 1A** shows that TRPC1, TRPC3, TRPC4, and TRPC6 are expressed in PASMCs and pulmonary artery endothelial cells (PAECs). As highlighted by the increased staining intensity, TRPC1, TRPC3, and TRPC6 appear overexpressed in PASMCs from remodeled PA in PAH patients. In contrast, TRPC4 staining intensity suggested increased TRPC4 expression in PAECs from PAH patients and not in PASMCs. As immunostaining is not quantitative, we performed immunoblot analyses on isolated human PA from control and PAH patients. Immunoblot showed a higher expression of TRPC1 and TRPC3 in isolated PAH-PA compared to the control condition, while TRPC4 and TRPC6 protein expressions were unchanged (**Figure 1B**). Since TRPC5 and TRPC7 mRNA were not detected in human pulmonary arteries[3], we did not investigate their role in PAH pathogenesis.

TRPC1, TRPC3, TRPC4 and TRPC6 contribute to exacerbated SOCE in PAH-hPASMCs

In PAH-hPASMCs, we found an increase in TRPC3 and TRPC6 protein expression and decreased expression of TRPC4. TRPC1 protein expression was unchanged in PAH-hPASMCs (**Figure 2A**).

Seventy-two hours after cells transfection with selective siRNA against each TRPC isoform (siTRPC1, siTRPC3, siTRPC4, or siTRPC6), each siRNAs used reduced the counterpart mRNA (**Figure 2B**) and protein (**Figure 2C**) without effect on other TRPC or Orai1 or STIM1 expression (**Figure S1**).

Then, we elicited the contribution of each TRPC on SOCE by depleting Ca^{2+} from the sarcoplasmic reticulum by applying 1 µmol/L thapsigargin (SERCA pump inhibitor) for 10 min in Ca^{2+} free medium and then by adding 2 mmol/L extracellular Ca^{2+} reached medium. We confirmed the 2-fold SOCE increase in PAH-hPASMCs compared to control-hPASMCs (**Figure 2D-E**), as recently described[4].

In control-PASMCs, only siTRPC1 decreased the SOCE (by 40 %) (**Figure 2D**). However, in PAH-hPASMCs, the knockdown of each TRPC isoform, TRPC1, TRPC3, TRPC4, or TRPC6, reduced SOCE amplitude by 50%, 50%, 60%, and 30%, respectively (**Figure 2E**).

TRPC channels are known to be involved in receptor-operated Ca^{2+} entry. We performed experiments to measure the contribution of each TRPC isoform on Ca^{2+} signaling mediated by GPCR activation induced by endothelin 1 (50 nmol/L) or histamine (10 µmol/L) stimulations (**Figure S2**). Ca^{2+} signaling induced by both stimulations was unchanged in control and PAH-hPASMCs (Figure S2A-C). Only the knockdown of TRPC1 reduced endothelin 1-mediated Ca^{2+} signaling (Figure S2B-D), while none of siTRPC affected histamine-induced Ca^{2+} signaling in PAH-PASMCs.

SOCE plays a crucial role in regulating calcineurin/NFAT activity, and we and others demonstrated exacerbated calcineurin activity in PAH-PASMCs[4]. We, therefore, measured the consequence of TRPC knockdown on calcineurin activity. We found that only TRPC3 knockdown reduced calcineurin activity in PAH-hPASMCs, indicating that increased TRPC3 expression/function contributes to calcineurin over-activity in PAH-PASMCs (**Figure 2F**).

To understand the increase of TRPC3 and TRPC6 in PAH-PASMCs, we evaluated the contribution of two major transcription factors involved in PAH pathogenesis, NFAT, and NF-kB, using selective pharmacological inhibitors. TRPC3 protein expression was unchanged in PAH-PASMCs treated with NFAT inhibitor (MCV1), while the treatment with NF-kB inhibitor (PDTC) reduced TRPC3 expression in PAH-hPASMCs (**Figure 2G**). The opposite effect was observed for TRPC6. Indeed, TRPC6 expression was decreased with MCV1 treatment but unchanged with PDTC treatment (**Figure 2H**). NFAT or NF-kB inhibition did not affect TRPC1 protein expression, while NF-kB inhibition reduced TRPC4 protein expression (**Figure S3A-B**). The selective inhibition of HIF1-α (LW6) did not change TRPC3 and TRPC6 expression in PAH-hPASMCs (**Figure S3C**).

TRPC channels contribute to the exacerbated proliferative phenotype of PAH-hPASMCs

We studied the contribution of each TRPC in control and PAH-hPASMCs proliferation, migratory capacity, and apoptosis resistance. In control-hPASMCs, only TRPC1 knockdown decreased the proliferation (**Figure 3A**). Interestingly and in association with the contribution of all TRPC to SOCE of PAH-hPASMCs, the proliferative capacity of these cells was decreased by about 40% in siTRPC1 or siTRPC3 or siTRPC4, or siTRPC6 treated PAH-hPASMCs (**Figure 3B**). In correlation with the impact of each TRPC isoform in the regulation of PAH-hPASMCs proliferation, we found that siTRPC6 reduced the activation of P42/44 assessed by the level of P42/44 phosphorylation (**Figure 3C**). These

results could partly explain the overactivation in P42/44 already described in PAH-PASMCs[11]. No changes in the expression and activation of P42/44 were found in PAH-hPASMCs treated with siTRPC1 or siTRPC3, or siTRPC4 (**Figure S4A**). We also found increased cell cycle inhibitor $P21^{CIP1/Waf1}$ (P21) protein expression in PAH-hPASMCs treated with siTRPC3 or siTRPC4 (**Figure 3E**). This cell cycle inhibitor is repressed in PAH-PASMCs[11]. These results suggest that TRPC3 and TRPC4 contribute to the PAH-hPASMCs excessive proliferative phenotype by regulating P21. In addition, in siTRPC1 or siTRPC6 treated PAH-hPASMCs, we found an increase in the Cas9/proCaspase9 ratio, without any significant changes in siTRPC3 or siTRPC4 treated cells (**Figure 3E, Figure S4B**), suggesting that TRPC1 and TRPC6 contribute partly to the apoptosis resistance phenotype of PAH-hPASMCs.

TRPC1 and TRPC4 channels contribute to the aberrant migratory capacity of PAH-hPASMCs

As increased PASMC migration is a feature of PAH pathogenesis[4], we analysed the contribution of TRPC isoform to the migratory capacity of control-PASMCs and PAH-PASMCs. In control-PASMCs, only the knockdown of TRPC1 caused a decrease in cell migration. In contrast, the knockdown of TRPC1 or TRPC4 decreased the migratory capacity of PAH-PASMCs (**Figure 4A-B**), indicating that both channels are involved in enhanced PAH-hPASMCs migration.

Reduction of TRPC expression worsens staurosporine-induced apoptosis in PAH-hPASMCs

To evaluate the contribution of TRPC channels in the resistance to apoptosis of PAH-PASMCs, we exposed cells to 50 nmol/L staurosporine (an apoptosis inducer) overnight to perform Annexin V-Propidium iodide staining and detect cell apoptosis. As illustrated in **Figure 5**, in PAH-hPASMCs, the knockdown of TRPC1 or TRPC3 or TRPC4, or TRPC6 increased the number of Annexin V-positive cells and simultaneously decreased the number of live cells (**Figure 5A-C**). Moreover, in staurosporine-exposed PAH-hPASMCs transfected with siTRPC1 or siTRPC3, or siTRPC4 or siTRPC6, the Caspase9/proCaspase9 ratio was increased, indicating that their knockdown increases apoptosis via Caspase9 activation (**Figure 5D**).

Increased TRPC3 expression/function in PH- induced by MCT exposure in rats

We investigated the expression of each isoform in the lung from MCT-PH rats (3 weeks after PH induction). Contrary to humans, immunoblot analyses from lungs MCT-PH rats revealed unchanged TRPC1 protein expression and reduced TRPC4, TRPC5, and TRPC6 compared to control animals (**Figure S5**). In contrast, TRPC3 expression was increased in MCT-PH rats' lungs (**Figure 6A**). Similarly, to human lung tissues, immunofluorescent staining showed that TRPC3 was expressed in PASMCs from control and MCT-PH rats with a higher fluorescence intensity in pulmonary arteries from MCT-PH rats (**Figure 6B**).

Then, using Pyr3, a selective inhibitor of TRPC3[19] at 1 µmol/L, we evaluated the involvement of TRPC3 in SOCE of PASMCs isolated from MCT-PH rats. As shown in **Figure 6C-D**, TRPC3 pharmacological inhibition reduced SOCE in MCT-PASMCs and PAH-hPASMCs.

As PA vasoconstriction is a hallmark of human and experimental PAH, we evaluated the role of TRPC3 in regulating pulmonary arterial constriction. TRPC3 inhibition by Pyr3 (1 µmol/L) induced a shift to the right of the dose-response curve for thromboxane A2 receptor agonist (U46619 at 0.1 to 3 µmol/L), meaning that TRPC3 contributes to PA constriction induced by thromboxane A2 mimetics (**Figure 6E-F**).

In vivo, TRPC3 pharmacological inhibition reduces the development of MCT-induced PH in rats.

Since we found that TRPC3 over-expression/function contributes to aberrant PAH-hPASMCs phenotypes and that only TRPC3 is overexpressed in the lung of MCT-PH rats, we next measured the consequence of *in vivo* TRPC3 pharmacological inhibition on the severity of PH induced by MCT exposure (60 mg/kg). We administered Pyr3 or vehicle (DMSO) daily intraperitoneal injection at 1 mg/kg during the last week of PH induction (**Figure 7A**). In comparison with MCT+DMSO animals, in the MCT + Pyr3 group, we found an improvement of the RV hypertrophy evaluated by measuring the Fulton index (**Figure 7B**), a reduction of the RV systolic pressure (**Figure 7C**), an increase of the cardiac output (**Figure 7D**) as well as an improvement of the total pulmonary resistance (**Figure 7E**). Moreover, *in vivo,* TRPC3 inhibition reduced MCT-exposure-induced pulmonary vessel obstruction (**Figure 7G**). At the cardiac level, RV fibrosis (**Figure 7F**) and RV cardiomyocyte cross-section area (**Figure 7G**) were improved in MCT + Pyr3 group compared with MCT + DMSO group. All these results

417 demonstrate the benefit of pharmacological inhibition of TRPC3 in the PH experimental model induced
418 by MCT exposure.

DISCUSSION

In the present study, we provide evidence of the contribution of TRPC channel isoforms to the development of PAH-hPASMCs pathological phenotype. First, we found that PAH-hPASMCs overexpressed TRPC3 and TRPC6. Second, the use of specific siRNA demonstrated that TRPC1, TRPC3, TRPC4, or TRPC6 contribute to aberrant SOCE, exacerbated proliferation, and apoptosis resistance of PAH-hPASMCs. In contrast, TRPC1 and TRPC4 increased the migratory capacity of PAH-hPASMCs. Third, we found that only TRPC3 contributes to calcineurin/NFAT activity exacerbation in PAH-hPASMCs. Fourth, we showed that TRPC3 protein/function is pathologically increased in lungs from MCT-induced PH rats. Finally, *in vivo* "curative" administration of the TRPC3 inhibitor attenuated PH development in the MCT-PH model.

We confirmed that hPASMCs expressed TRPC1, TRPC3, TRPC4, and TRPC6 isoforms, as previously described[3], while TRPC1, TRPC3, TRPC4, TRPC5, and TRPC6 were expressed in rodent PASMCs[3,20]. TRPC1 was overexpressed in control-hPASMCs undergoing proliferation in association with increased SOCE, meaning that TRPC1 contributes to SOCE in control-hPASMCs[3]. In rat or human control-PASMCs, hypoxia exposure increased the expression of TRPC1 or TRPC6 in association with increased SOCE[21,22]. In rats exposed to chronic intermittent hypoxia, lung TRPC1, TRPC4, and TRPC6 protein expression was increased compared to rats under normoxia[23,24]. In CH-induced PH rats, the expression of TRPC1 and TRPC6 were increased in isolated PA, associated with increased SOCE[25]. Altogether these data suggest that hypoxia-inducible factor 1 alpha (HIF-1α) could regulate TRPC expression. However, we found that HIF-1α pharmacological inhibition had no impact on the expression of TRPC3 and TRPC6 in PAH-hPASMCs, indicating that increased HIF-1α activity in PAH[26] is not responsible for TRPC channel remodeling in PAH-hPASMCs. In iPAH-hPASMCs, the knockdown of TRPC6 reduced the hyperproliferative phenotype[27]. Here, we found in PAH-hPASMCs an increased expression of TRPC1, TRPC3, and TRPC6, contributing equally to increased SOCE.

In PAH-hPASMCs, we found that NF-kB and NFAT signaling partly control the increased TRPC3 and TRPC6 protein expression, respectively. In contrast to neonatal rat ventricular myocytes, where it has been demonstrated that TRPC3 expression is regulated through a calcineurin/NFAT mechanism (and not by NF-kB) and that TRPC3 function contributes to calcineurin activity[28], we found in PAH-hPASMCs that calcineurin/NFAT did not control TRPC3 expression. However, the TRPC3 function

partly controlled calcineurin overactivity in PAH-hPASMCs. Unlike TRPC3, we highlighted that TRPC6 overexpression in PAH-hPASMCs is regulated by calcineurin/NFAT and not by NF-kB, as previously described in rodent cardiomyocytes[29]. However, in PAH-hPASMCs, the TRPC6 function did not influence the calcineurin function**.** In cardiomyocytes, we found that aldosterone exposure mediates TRPC upregulation[30,31]. As aldosterone contributes to PAH pathogenesis in humans[32] and experimental PH[33], we propose that aldosterone overproduction could enhance TRPC channels expression in PAH.

An additional mechanism can explain the overexpression/overactivity of TRPC6 in PAH. We recently observed a reduced expression of the chloride and bicarbonate transporter CFTR (cystic fibrosis transmembrane regulator) in PAH-hPASMCs[18], which is known to be functionally and physically coupled to TRPC6[34,35]. In human airway epithelial cells, the loss of CFTR enhances TRPC6 expression and function[34], observed in mice pulmonary vasculature contributing to hypoxic vasoconstriction[35], suggesting overexpression/overactivity of TRPC6 in PAH could be related to CFTR loss in PAH-hPASMCs.

To be fully functional, TRPC channels can form homo-tetrameric channels or hetero-tetrameric channels like TRPC1/3, TRPC1/4, TRPC1/5, TRPC3/4, TRPC4/5, and TRPC1/4/5[3]. The inhibition of TRPC channels by pharmacological or knockdown approaches indicates that TRPC1, TRPC4, and TRPC5 participate in SOCE in several cell types[36]. However, TRPC channels activation mainly occurs following the activation of Gq-coupled receptor and tyrosine kinases receptor, coupled to phospholipase C (PLC) *via* inositol trisphosphate IP_3-dependent Ca^{2+} release from the endoplasmic reticulum or through DAG (diacylglycerol) synthesis. Ca^{2+} could also indirectly regulate TRPC channel function by activating calmodulin and other Ca^{2+}-binding proteins or phosphatidylinositol-4,5-bisphosphate (PIP_2). Protein kinase C (PKC) can activate TRPC3 in human endothelial cells during ER Ca^{2+} depletion induced by thapsigargin stimulation [37]. STIM1 interacts (directly or indirectly) with TRPC channels (except TRPC7), conferring to TRPC a SOCE function[38,39]. It has also been described that TRPC1 function could be dependent on the Orai1-mediated Ca^{2+} entry, permitting the recruitment of TRPC1 into the plasma membrane[40]. We found that STIM1 and Orai1 expressions were unaffected by the knockdown of TRPC. However, we do not entirely exclude that reduced TRPC expression alters STIM1/Orai1 clustering.

In the context of PAH, where several growth factors (Transforming growth factor beta, Platelet-derived growth factor, Epidermal Growth Factor) or proangiogenic molecules (Endothelin1, Thromboxane A2) are known to be overexpressed, we could hypothesize that all cited molecules could activate TRPC channels by inducing endoplasmic reticulum SR Ca^{2+} depletion, DAG production, PKC activation, generating intracellular Ca^{2+} elevation. Here we found that all expressed TRPC in hPASMCs are involved in SOCE of PAH-hPASMCs. In contrast, only TRPC1 and TRPC4 are involved in SOCE of control-hPASMCs suggesting dysregulation of a protein complex or activation mechanisms, which need to be elucidated in further study.

In rat models, TRPC1 overexpression has been demonstrated to enhance PA vasoconstriction[41], suggesting that TRPC1-mediated SOCE regulates PASMC contraction. In rat aortic smooth muscle cells, TRPC1 is complexed to the KCa channel (Ca^{2+}-sensitive K^+ channels), promoting TRPC1 Ca^{2+} entry and then membrane hyperpolarisation. Plasma membrane hyperpolarisation mediated by the TRPC1-KCa complex could limit smooth muscle cell contraction by reducing membrane depolarization[42]. *Trpc6* deficiency in mice impaired the contractile capacity of mesangial cells[43]. TRPC3 inhibitor application mediates mesenteric artery vasodilatation, suggesting that TRPC3 function contributes to mesenteric constriction regulation[44]. Here, we found that selective TRPC3 pharmacological inhibition reduced the contractile capacity mediated by thromboxane A2, suggesting that TRPC3 exacerbated function in PAH-PASMCs could contribute to PA vasoconstriction.

Even though PAH patients died due to RV failure, RV failure is understudied compared to left ventricular failure (LVF). Nevertheless, many studies demonstrated that TRPC channels are crucial for Ca^{2+} mishandling in LVF[45]. Indeed, a considerable amount of knowledge obtained in experimental models demonstrated the crucial role of each TRPC isoform in the development of LV hypertrophy (LVH) or LVF[45]. In humans, failing hearts increase TRPC1, TRPC5, and TRPC6 expression[45], suggesting that TRPC channels are also involved in human heart failure. In most cases, TRPC upregulation leads to increasing SOCE that activates the calcineurin/NFAT pathway and/or Calmodulin Kinase II pathway or the NF-κB pathway influencing ventricular remodeling[46]. Selective pharmacological inhibition of TRPC3 and TRPC6 has been proposed to attenuate LVH and improve LV function induced by pressure overload in mice[19,47]. In the RV, only a few studies investigated the implication of SOCE in RV remodeling. We found a significant reduction of CO in MCT-DMSO rats,

indicating that these animals developed heart failure. We showed an improvement of CO after TRPC3 selective inhibition, explained by the reduction of pulmonary vascular narrowing and direct action on the TRPC3 channels expressed in RV cardiomyocytes[48]. In RVF induced by MCT in rats, the mRNA level of *Trpc1* decreased, while the mRNA level of Trpc6 increased[49]. At the protein level, we found an upregulation of TRPC1/TRPC4 expression and of the long STIM1 in RVF induced by MCT exposure in rats correlated with an increased SOC current, contributing to the RV remodeling during hypertrophic stress[48]. In this previous study, TRPC3 protein expression was unchanged in RV from MCT-PH rats[48]. In the present study, we found that *in vivo* inhibition of TRPC3 improved RV hypertrophy and systolic pressure in MCT-PH rat models, explained by a reduction in pulmonary vascular remodeling and, to some extent, by the direct action of TRPC3 inhibition on RV myocyte function.

By preventing pulmonary vessel remodeling induced by CH exposure, double *trpc1/trpc6* knockout mice are protected against PH[50], indicating that TRPC1 and TRPC6 are essential for CH-induced PH in mice. Moreover, *in vivo*, administration of siRNA against TRPC1 in CH-exposed mice reduces pulmonary arterial remodeling and RV systolic pressure[51]. Furthermore, *trpc1*$^{-/-}$ mice developed partial protection against PH in response to CH compared to wild-type mice[52]. *Trpc4*$^{-/-}$ rats exposed to Sugen/hypoxia exhibited similar hemodynamic parameters to wild-type rats, but *Trpc4*$^{-/-}$ rats showed a significant survival benefit, preserving cardiac output[53]. *In vivo* TRPC6 inhibition with BI-749237 compound reduced PH phenotype in mice exposed to chronic hypoxia[54], suggesting that TRPC6 could also be a potential target in PAH. Using the siRNA strategy, we found that TRPC3 inhibition reduced several pathological phenotypes of PAH-hPASMCs *in vitro*, including aberrant proliferation, exacerbated migration, and apoptosis resistance. Finally, our present results revealed that *in vivo* "curative" inhibition of TRPC3 reduced the development of PH in rats MCT-PH model. These data highlight that targeting the TRPC3 function could be a promising strategy for treating PAH.

Indeed, this study has some limitations. First, Pyr3 has been described to selectively and directly inhibit TRPC3 channels. Since the IC_{50} of Pyr3 for TRPC3 is 700 nmol/L, we used in the present study PYR3 at 1 µmol/L for our *in vivo* experiments to avoid potential side effects. Indeed, it was documented that at higher concentration (3 µmol/L), Pyr3 can also inhibit TRPC6[19]. At 3 µmol/L, Pyr3 was also suggested to reduce Orai1 Ca^{2+} channel function[55]. Since Orai1 or TRPC6 inhibition reduces

experimental PH[4,54], we cannot discriminate whether Pyr3 *in vivo* exposure protects rats from PH through the Orai1 and/or TRPC6 function. However, we found that Pyr3 at 1 µmol/L has similar effects on SOCE in PAH-hPASMCs compared with siRNA directed against TRPC3 in transfected PAH-hPASMCs. Moreover, despite significant evolution in the selectivity of pharmacological molecules targeting TRPC, we were limited in using a selective inhibitor of each TRPC isoform since we found in the present study that all TRPC isoforms could be an interesting target to reduce PAH-hPASMCs dysfunctions.

In conclusion, our findings prove that all TRPC isoforms contribute to PAH pathogenesis by regulating the PAH-PASMC phenotypes, such as hyper-proliferation, apoptosis resistance, excessive migration, and contraction. Our data reveal that pharmacological inhibition of TRPC3 may be a relevant approach to decrease pulmonary vascular remodeling in PAH.

DATA AVAILABILITY

The authors declare that all supporting data are available within the article and its Online Data Supplement.

SUPPLEMENTAL DATA

All Supplemental Material is available 10.6084/m9.figshare.23145740.

Supplemental Table 1

Supplemental Table 2

Supplemental Table 3

Supplemental Fig. S1

Supplemental Fig. S2

Supplemental Fig. S3

Supplemental Fig. S4

Supplemental Fig. S5

ACKNOWLEDGMENTS

The authors thank Yvonne Dutheil from INSERM U999 and Hopital Marie Lannelongue for all her help.

GRANTS

This study was supported by grants from the French National Institute for Health and Medical Research (INSERM), the Université Paris-Saclay, the Marie Lannelongue Hospital, and the French National Agency for Research (ANR) (grant no. ANR-18-CE14-0023 (KAPAH). B.M. and A. SM-W are supported by the Therapeutic Innovation Doctoral School (ED569).

DISCLOSURES

MH and DM have relationships with drug companies, including Actelion, Bayer, GSK, Novartis, and Pfizer. In addition to being investigators in trials involving these companies, other relationships include consultancy services and memberships to scientific advisory boards. The other authors have no conflicts of interest to declare.

AUTHOR CONTRIBUTIONS

B.M, A.S-M-W, V.C, and F.A. participated in the research design. B.M, A.S-M-W, M.D, L.P, C. E-J, V.C, and F.A. conducted the experiments and analysed the data. All authors drafted the manuscript for important intellectual content the manuscript. All authors reviewed and revised the final version and approved the manuscript submission.

REFERENCES

1. Humbert M, Guignabert C, Bonnet S, Dorfmüller P, Klinger JR, Nicolls MR, Olschewski AJ, Pullamsetti SS, Schermuly RT, Stenmark KR, Rabinovitch M. Pathology and pathobiology of pulmonary hypertension: state of the art and research perspectives. *Eur Respir J* 2019;**53**:1801887.

2. Simonneau G, Montani D, Celermajer DS, Denton CP, Gatzoulis MA, Krowka M, Williams PG, Souza R. Haemodynamic definitions and updated clinical classification of pulmonary hypertension. *Eur Respir J* 2019;**53**.

3. Masson B, Montani D, Humbert M, Capuano V, Antigny F. Role of Store-Operated Ca2+ Entry in the Pulmonary Vascular Remodeling Occurring in Pulmonary Arterial Hypertension. *Biomolecules* 2021;**11**:1781.

4. Masson B, Le Ribeuz H, Sabourin J, Laubry L, Woodhouse E, Foster R, Ruchon Y, Dutheil M, Boët A, Ghigna M-R, De Montpreville V, Mercier O, Beech DJ, Benitah J-P, Bailey MA, Humbert M, Montani D, Capuano V, Antigny F. Orai1 Inhibitors as Potential Treatments for Pulmonary Arterial Hypertension. *Circ Res* 2022:101161CIRCRESAHA122321041.

5. Earley S, Brayden JE. Transient receptor potential channels in the vasculature. *Physiol Rev* 2015;**95**:645–690.

6. Vannier B, Peyton M, Boulay G, Brown D, Qin N, Jiang M, Zhu X, Birnbaumer L. Mouse trp2, the homologue of the human trpc2 pseudogene, encodes mTrp2, a store depletion-activated capacitative Ca2+ entry channel. *Proc Natl Acad Sci U S A* 1999;**96**:2060–2064.

7. Ruhle B, Trebak M. Emerging roles for native Orai Ca2+ channels in cardiovascular disease. *Curr Top Membr* 2013;**71**:209–235.

8. Yu Y, Keller SH, Remillard CV, Safrina O, Nicholson A, Zhang SL, Jiang W, Vangala N, Landsberg JW, Wang J-Y, Thistlethwaite PA, Channick RN, Robbins IM, Loyd JE, Ghofrani HA, Grimminger F, Schermuly RT, Cahalan MD, Rubin LJ, Yuan JX-J. A functional single-nucleotide polymorphism in the TRPC6 gene promoter associated with idiopathic pulmonary arterial hypertension. *Circulation* 2009;**119**:2313–2322.

9. Xia Y, Yang X-R, Fu Z, Paudel O, Abramowitz J, Birnbaumer L, Sham JSK. Classical transient receptor potential 1 and 6 contribute to hypoxic pulmonary hypertension through differential regulation of pulmonary vascular functions. *Hypertens Dallas Tex 1979* 2014;**63**:173–180.

10. Malkmus K, Brosien M, Knoepp F, Schaffelhofer L, Grimminger F, Rummel C, Gudermann T, Dietrich A, Birnbaumer L, Weissmann N, Kraut S. Deletion of classical transient receptor potential 1, 3 and 6 alters pulmonary vasoconstriction in chronic hypoxia-induced pulmonary hypertension in mice. *Front Physiol* 2022;**13**:1080875.

11. Sankhe S, Manousakidi S, Antigny F, Arthur Ataam J, Bentebbal S, Ruchon Y, Lecerf F, Sabourin J, Price L, Fadel E, Dorfmüller P, Eddahibi S, Humbert M, Perros F, Capuano V. T-type Ca2+channels elicit pro-proliferative and anti-apoptotic responses through impaired PP2A/Akt1 signaling in PASMCs from patients with pulmonary arterial hypertension. *Biochim Biophys Acta* 2017;**1864**:1631–1641.

12. Lambert M, Capuano V, Boet A, Tesson L, Bertero T, Nakhleh MK, Remy S, Anegon I, Pechoux C, Hautefort A, Rucker-Martin C, Manoury B, Domergue V, Mercier O, Girerd B, Montani D, Perros F, Humbert M, Antigny F. Characterization of *Kcnk3* -Mutated Rat, a Novel Model of Pulmonary Hypertension. *Circ Res* 2019;**125**:678–695.

13. Eddahibi S, Humbert M, Fadel E, Raffestin B, Darmon M, Capron F, Simonneau G, Dartevelle P, Hamon M, Adnot S. Serotonin transporter overexpression is responsible for pulmonary artery smooth muscle hyperplasia in primary pulmonary hypertension. *J Clin Invest* 2001;**108**:1141–1150.

14. Le Ribeuz H, Masson B, Capuano V, Dutheil M, Gooroochurn H, Boët A, Ghigna M-R, De Montpreville V, Girerd B, Lambert M, Mercier O, Chung WK, Humbert M, Montani D, Antigny F. SUR1 as a New Therapeutic Target for Pulmonary Arterial Hypertension. *Am J Respir Cell Mol Biol* 2022.

15. Le Ribeuz H, Courboulin A, Ghigna M-R, Lambert M, Hautefort A, Humbert M, Montani D, Cohen-Kaminsky S, Perros F, Antigny F. In vivo miR-138-5p inhibition alleviates monocrotaline-induced pulmonary hypertension and normalizes pulmonary KCNK3 and SLC45A3 expression. *Respir Res* 2020;**21**:186.

16. Lambert M, Mendes-Ferreira P, Ghigna M-R, LeRibeuz H, Adão R, Boet A, Capuano V, Rucker-Martin C, Brás-Silva C, Quarck R, Domergue V, Vachiéry J-L, Humbert M, Perros F, Montani D, Antigny F. Kcnk3 dysfunction exaggerates the development of pulmonary hypertension induced by left ventricular pressure overload. *Cardiovasc Res* 2021;**117**:2474–2488.

17. Lambert M, Boet A, Rucker-Martin C, Mendes-Ferreira P, Capuano V, Hatem S, Adão R, Brás-Silva C, Hautefort A, Michel J-B, Dorfmuller P, Fadel E, Kotsimbos T, Price L, Jourdon P, Montani D, Humbert M, Perros F, Antigny F. Loss of KCNK3 is a hallmark of RV hypertrophy/dysfunction associated with pulmonary hypertension. *Cardiovasc Res* 2018;**114**:880–893.

18. Le Ribeuz H, To L, Ghigna M-R, Martin C, Nagaraj C, Dreano E, Rucker-Martin C, Girerd B, Bouliguan J, Pechoux C, Lambert M, Boet A, Issard J, Mercier O, Hoetzenecker K, Manoury B, Becq F, Burgel P-R, Cottart C-H, Olschewski A, Sermet-Gaudelus I, Perros F, Humbert M, Montani D, Antigny F. Involvement of CFTR in the pathogenesis of pulmonary arterial hypertension. *Eur Respir J* 2021:2000653.

19. Kiyonaka S, Kato K, Nishida M, Mio K, Numaga T, Sawaguchi Y, Yoshida T, Wakamori M, Mori E, Numata T, Ishii M, Takemoto H, Ojida A, Watanabe K, Uemura A, Kurose H, Morii T, Kobayashi T, Sato Y, Sato C, Hamachi I, Mori Y. Selective and direct inhibition of TRPC3 channels underlies biological activities of a pyrazole compound. *Proc Natl Acad Sci U S A* 2009;**106**:5400–5405.

20. Lambert M, Capuano V, Olschewski A, Sabourin J, Nagaraj C, Girerd B, Weatherald J, Humbert M, Antigny F. Ion Channels in Pulmonary Hypertension: A Therapeutic Interest? *Int J Mol Sci* 2018;**19**.

21. Ng LC, Airey JA, Hume JR. The contribution of TRPC1 and STIM1 to capacitative Ca(2+) entry in pulmonary artery. *Adv Exp Med Biol* 2010;**661**:123–135.

22. Lu W, Wang J, Shimoda LA, Sylvester JT. Differences in STIM1 and TRPC expression in proximal and distal pulmonary arterial smooth muscle are associated with differences in Ca2+ responses to hypoxia. *Am J Physiol Lung Cell Mol Physiol* 2008;**295**:L104-113.

23. Castillo-Galán S, Arenas GA, Reyes RV, Krause BJ, Iturriaga R. Stim-activated TRPC-ORAI channels in pulmonary hypertension induced by chronic intermittent hypoxia. *Pulm Circ* 2020;**10**:13–22.

24. Castillo-Galán S, Arenas GA, Iturriaga R. Contribution of STIM-Activated TRPC-ORAI Channels in Pulmonary Hypertension Induced by Chronic Sustained and Intermittent Hypoxia. *Curr Vasc Pharmacol* 2022;**20**:272–283.

25. Lin M-J, Leung GPH, Zhang W-M, Yang X-R, Yip K-P, Tse C-M, Sham JSK. Chronic hypoxia-induced upregulation of store-operated and receptor-operated Ca2+ channels in pulmonary arterial smooth muscle cells: a novel mechanism of hypoxic pulmonary hypertension. *Circ Res* 2004;**95**:496–505.

26. Bonnet S, Michelakis ED, Porter CJ, Andrade-Navarro MA, Thébaud B, Bonnet S, Haromy A, Harry G, Moudgil R, McMurtry MS, Weir EK, Archer SL. An abnormal mitochondrial-hypoxia inducible factor-1alpha-Kv channel pathway disrupts oxygen sensing and triggers pulmonary arterial hypertension in fawn hooded rats: similarities to human pulmonary arterial hypertension. *Circulation* 2006;**113**:2630–2641.

27. Yu Y, Fantozzi I, Remillard CV, Landsberg JW, Kunichika N, Platoshyn O, Tigno DD, Thistlethwaite PA, Rubin LJ, Yuan JX-J. Enhanced expression of transient receptor potential channels in idiopathic pulmonary arterial hypertension. *Proc Natl Acad Sci U S A* 2004;**101**:13861–13866.

28. Bush EW, Hood DB, Papst PJ, Chapo JA, Minobe W, Bristow MR, Olson EN, McKinsey TA. Canonical transient receptor potential channels promote cardiomyocyte hypertrophy through activation of calcineurin signaling. *J Biol Chem* 2006;**281**:33487–33496.

29. Kuwahara K, Wang Y, McAnally J, Richardson JA, Bassel-Duby R, Hill JA, Olson EN. TRPC6 fulfills a calcineurin signaling circuit during pathologic cardiac remodeling. *J Clin Invest* 2006;**116**:3114–3126.

30. Bartoli F, Moradi Bachiller S, Antigny F, Bedouet K, Gerbaud P, Sabourin J, Benitah J-P. Specific Upregulation of TRPC1 and TRPC5 Channels by Mineralocorticoid Pathway in Adult Rat Ventricular Cardiomyocytes. *Cells* 2019;**9**:E47.

31. Sabourin J, Bartoli F, Antigny F, Gomez AM, Benitah J-P. Transient Receptor Potential Canonical (TRPC)/Orai1-dependent Store-operated Ca2+ Channels: NEW TARGETS OF ALDOSTERONE IN CARDIOMYOCYTES. *J Biol Chem* 2016;**291**:13394–13409.

32. Maron BA, Opotowsky AR, Landzberg MJ, Loscalzo J, Waxman AB, Leopold JA. Plasma aldosterone levels are elevated in patients with pulmonary arterial hypertension in the absence of left ventricular heart failure: a pilot study. *Eur J Heart Fail* 2013;**15**:277–283.

33. Tu L, Thuillet R, Perrot J, Ottaviani M, Ponsardin E, Kolkhof P, Humbert M, Viengchareun S, Lombès M, Guignabert C. Mineralocorticoid Receptor Antagonism by Finerenone Attenuates Established Pulmonary Hypertension in Rats. *Hypertens Dallas Tex 1979* 2022;**79**:2262–2273.

34. Antigny F, Norez C, Dannhoffer L, Bertrand J, Raveau D, Corbi P, Jayle C, Becq F, Vandebrouck C. Transient Receptor Potential Canonical Channel 6 Links Ca^{2+} Mishandling to Cystic Fibrosis Transmembrane Conductance Regulator Channel Dysfunction in Cystic Fibrosis. *Am J Respir Cell Mol Biol* 2011;**44**:83–90.

35. Tabeling C, Yu H, Wang L, Ranke H, Goldenberg NM, Zabini D, Noe E, Krauszman A, Gutbier B, Yin J, Schaefer M, Arenz C, Hocke AC, Suttorp N, Proia RL, Witzenrath M, Kuebler WM. CFTR and sphingolipids mediate hypoxic pulmonary vasoconstriction. *Proc Natl Acad Sci U S A* 2015;**112**:E1614–E1623.

36. Lopez JJ, Jardin I, Sanchez-Collado J, Salido GM, Smani T, Rosado JA. TRPC Channels in the SOCE Scenario. *Cells* 2020;**9**:126.

37. Antigny F, Jousset H, König S, Frieden M. Thapsigargin activates Ca^{2}+ entry both by store-dependent, STIM1/Orai1-mediated, and store-independent, TRPC3/PLC/PKC-mediated pathways in human endothelial cells. *Cell Calcium* 2011;**49**:115–127.

38. Choi S, Maleth J, Jha A, Lee KP, Kim MS, So I, Ahuja M, Muallem S. The TRPCs-STIM1-Orai interaction. *Handb Exp Pharmacol* 2014;**223**:1035–1054.

39. Zeng W, Yuan JP, Kim MS, Choi YJ, Huang GN, Worley PF, Muallem S. STIM1 gates TRPC channels, but not Orai1, by electrostatic interaction. *Mol Cell* 2008;**32**:439–448.

40. Cheng KT, Liu X, Ong HL, Swaim W, Ambudkar IS. Local Ca^2+ entry via Orai1 regulates plasma membrane recruitment of TRPC1 and controls cytosolic Ca^2+ signals required for specific cell functions. *PLoS Biol* 2011;**9**:e1001025.

41. Kunichika N, Yu Y, Remillard CV, Platoshyn O, Zhang S, Yuan JX-J. Overexpression of TRPC1 enhances pulmonary vasoconstriction induced by capacitative Ca2+ entry. *Am J Physiol Lung Cell Mol Physiol* 2004;**287**:L962-969.

42. Kwan H-Y, Shen B, Ma X, Kwok Y-C, Huang Y, Man Y-B, Yu S, Yao X. TRPC1 Associates With BKCa Channel to Form a Signal Complex in Vascular Smooth Muscle Cells. *Circ Res* 2009;**104**:670–678.

43. Li W, Ding Y, Smedley C, Wang Y, Chaudhari S, Birnbaumer L, Ma R. Increased glomerular filtration rate and impaired contractile function of mesangial cells in TRPC6 knockout mice. *Sci Rep* 2017;**7**:4145.

44. Álvarez-Miguel I, Cidad P, Pérez-García MT, López-López JR. Differences in TRPC3 and TRPC6 channels assembly in mesenteric vascular smooth muscle cells in essential hypertension. *J Physiol* 2017;**595**:1497–1513.

45. Sabourin J, Beauvais A, Luo R, Montani D, Benitah J-P, Masson B, Antigny F. The SOCE Machinery: An Unbalanced Knowledge between Left and Right Ventricular Pathophysiology. *Cells* 2022;**11**:3282.

46. Wen H, Gwathmey JK, Xie L-H. Role of Transient Receptor Potential Canonical Channels in Heart Physiology and Pathophysiology. *Front Cardiovasc Med* 2020;**7**:24.

47. Seo K, Rainer PP, Shalkey Hahn V, Lee D, Jo S-H, Andersen A, Liu T, Xu X, Willette RN, Lepore JJ, Marino JP, Birnbaumer L, Schnackenberg CG, Kass DA. Combined TRPC3 and TRPC6 blockade by selective small-molecule or genetic deletion inhibits pathological cardiac hypertrophy. *Proc Natl Acad Sci U S A* 2014;**111**:1551–1556.

48. Sabourin J, Boet A, Rucker-Martin C, Lambert M, Gomez A-M, Benitah J-P, Perros F, Humbert M, Antigny F. Ca2+ handling remodeling and STIM1L/Orai1/TRPC1/TRPC4 upregulation in monocrotaline-induced right ventricular hypertrophy. *J Mol Cell Cardiol* 2018;**118**:208–224.

49. Benoist D, Stones R, Drinkhill MJ, Benson AP, Yang Z, Cassan C, Gilbert SH, Saint DA, Cazorla O, Steele DS, Bernus O, White E. Cardiac arrhythmia mechanisms in rats with heart failure induced by pulmonary hypertension. *Am J Physiol Heart Circ Physiol* 2012;**302**:H2381-2395.

50. Xia Y, Yang X-R, Fu Z, Paudel O, Abramowitz J, Birnbaumer L, Sham JSK. TRPC1 and TRPC6 Contribute to Hypoxic Pulmonary Hypertension through Differential Regulation of Pulmonary Vascular Functions RR. *Hypertension* 2014;**63**:173–180.

51. Reducing TRPC1 Expression through Liposome-Mediated siRNA Delivery Markedly Attenuates Hypoxia-Induced Pulmonary Arterial Hypertension in a Murine Model - PubMedhttps://pubmed-ncbi-nlm-nih-gov.proxy.insermbiblio.inist.fr/25587286/ (28 November 2022)

52. Malczyk M, Veith C, Fuchs B, Hofmann K, Storch U, Schermuly RT, Witzenrath M, Ahlbrecht K, Fecher-Trost C, Flockerzi V, Ghofrani HA, Grimminger F, Seeger W, Gudermann T, Dietrich A, Weissmann N. Classical transient receptor potential channel 1 in hypoxia-induced pulmonary hypertension. *Am J Respir Crit Care Med* 2013;**188**:1451–1459.

53. Alzoubi A, Almalouf P, Toba M, O'Neill K, Qian X, Francis M, Taylor MS, Alexeyev M, McMurtry IF, Oka M, Stevens T. TRPC4 inactivation confers a survival benefit in severe pulmonary arterial hypertension. *Am J Pathol* 2013;**183**:1779–1788.

54. Jain PP, Lai N, Xiong M, Chen J, Babicheva A, Zhao T, Parmisano S, Zhao M, Paquin C, Matti M, Powers R, Balistrieri A, Kim NH, Valdez-Jasso D, Thistlethwaite PA, Shyy JY-J, Wang J, Garcia JGN, Makino A, Yuan JX-J. TRPC6, a therapeutic target for pulmonary hypertension. *Am J Physiol Lung Cell Mol Physiol* 2021;**321**:L1161–L1182.

55. Schleifer H, Doleschal B, Lichtenegger M, Oppenrieder R, Derler I, Frischauf I, Glasnov TN, Kappe CO, Romanin C, Groschner K. Novel pyrazole compounds for pharmacological discrimination between receptor-operated and store-operated Ca(2+) entry pathways. *Br J Pharmacol* 2012;**167**:1712–1722.

Figure Legends

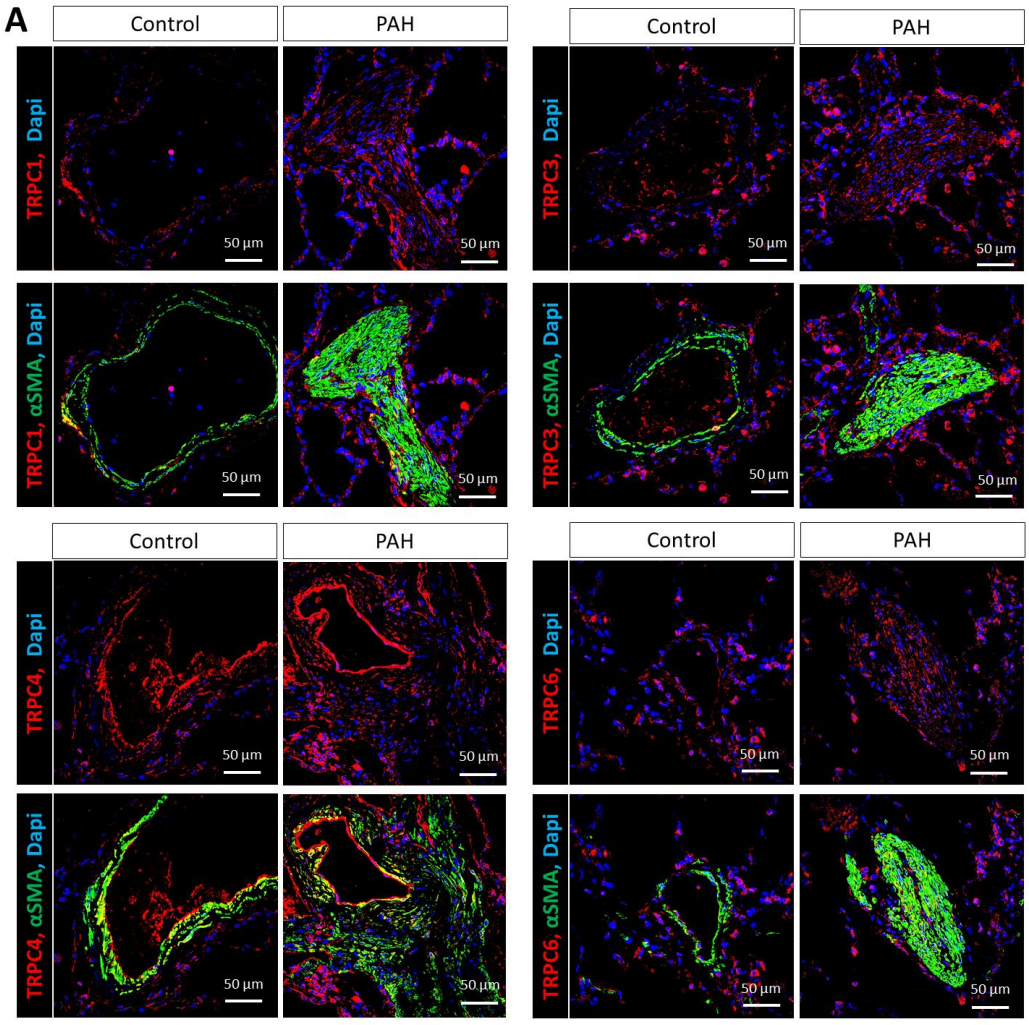
A
Control
PAH
TRPC1, Dapi
TRPC1, αSMA, Dapi
TRPC3, Dapi
TRPC3, αSMA, Dapi
TRPC4, Dapi
TRPC4, αSMA, Dapi
TRPC6, Dapi
TRPC6, αSMA, Dapi
50 µm

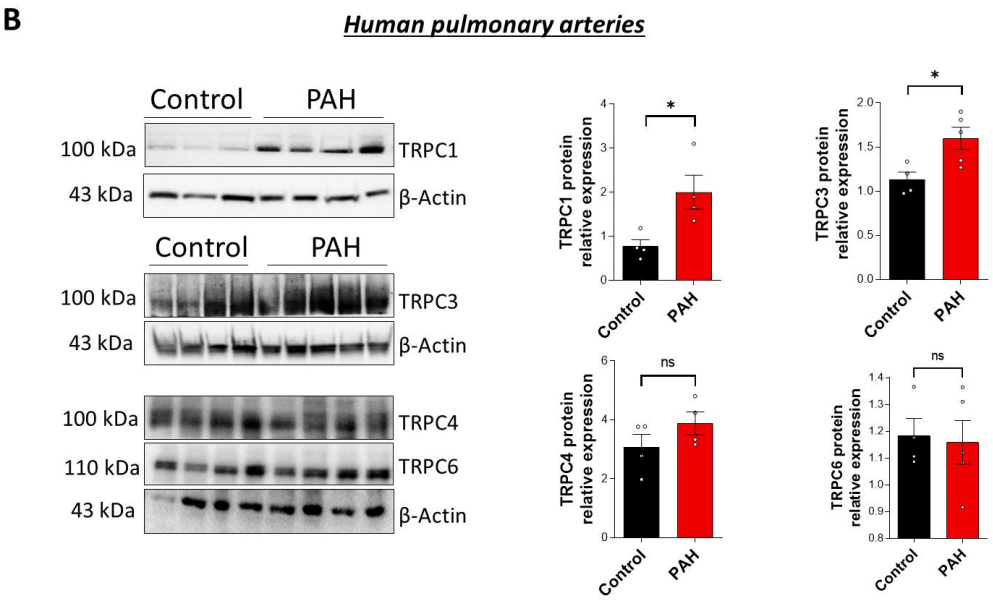
B
Human pulmonary arteries
Control
PAH
100 kDa
43 kDa
110 kDa
TRPC1
TRPC3
TRPC4
TRPC6
β-Actin
TRPC1 protein relative expression
TRPC3 protein relative expression
TRPC4 protein relative expression
TRPC6 protein relative expression
*
ns

Figure 1

Figure 1: Increased expression of TRPC1 and TRPC3 in pulmonary arteries (PA) isolated from patients with pulmonary arterial hypertension (PAH). (A) Expression and localization of TRPC1, TRPC3, TRPC4, and TRPC6 by immunofluorescence staining on paraffin-embedded lung sections from control and PAH patients (Dapi staining (blue), TRPC staining (red) and αSMA staining (green)). Bar graph = 50 µm. (B) Immunoblot and quantification of TRPC1 (n=4 patients), TRPC3 (n=5 patients), TRPC4 (n=4 patients), or TRPC6 (n=5 patients) in pulmonary arteries from control and PAH patients. Experiments presented in panel B were analysed using the Mann-Whitney test. ns = non-significant; *$P< 0.05$.

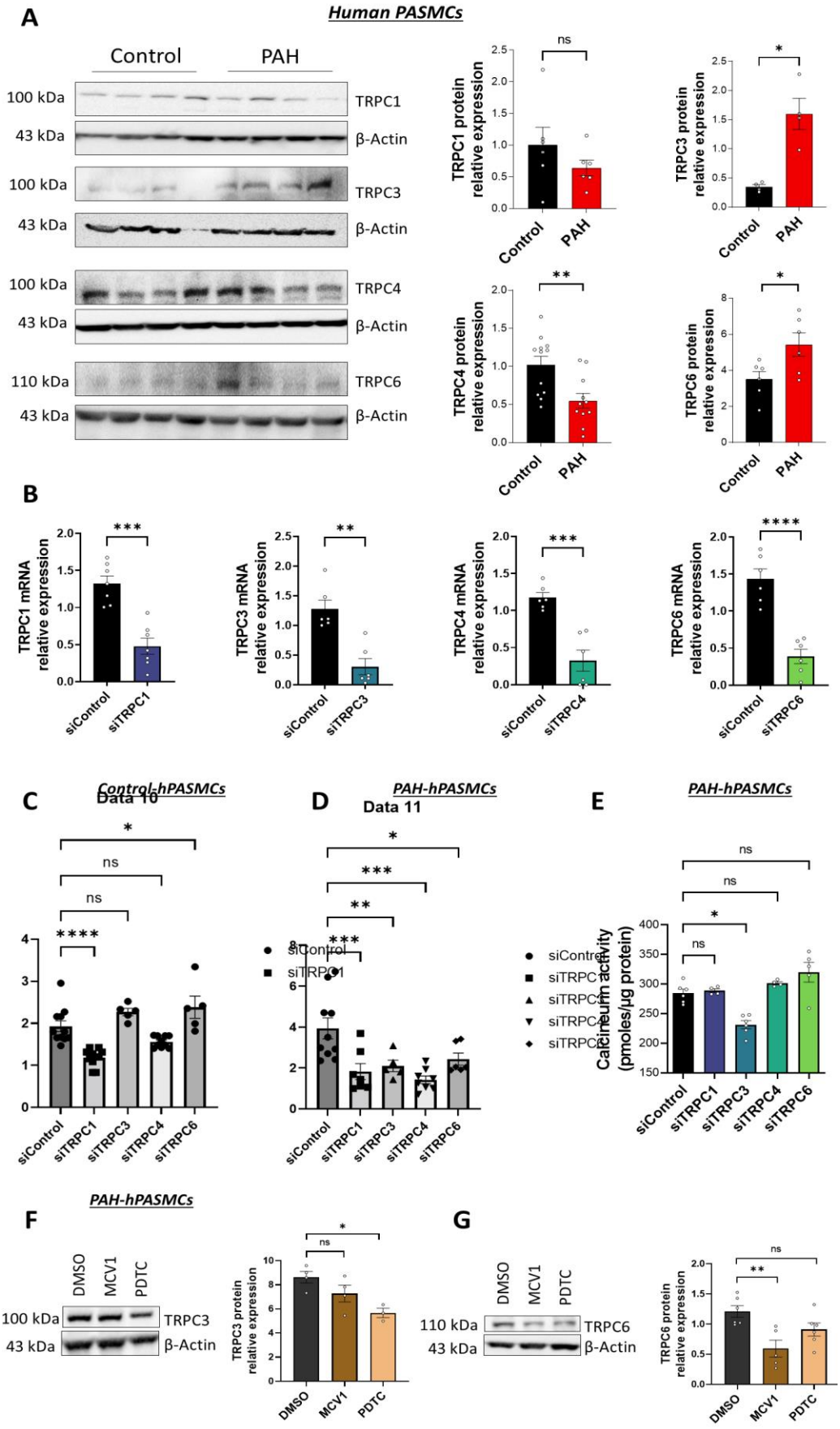
A
Human PASMCs
Control
PAH
100 kDa
TRPC1
43 kDa
β-Actin
100 kDa
TRPC3
43 kDa
β-Actin
100 kDa
TRPC4
43 kDa
β-Actin
110 kDa
TRPC6
43 kDa
β-Actin
TRPC1 protein relative expression
TRPC3 protein relative expression
TRPC4 protein relative expression
TRPC6 protein relative expression
ns
*
**
Control
PAH
B
TRPC1 mRNA relative expression
TRPC3 mRNA relative expression
TRPC4 mRNA relative expression
TRPC6 mRNA relative expression
***
**
***
****
siControl
siTRPC1
siTRPC3
siTRPC4
siTRPC6
C
Control-hPASMCs
Data 10
D
PAH-hPASMCs
Data 11
E
PAH-hPASMCs
Calcineurin activity (pmoles/µg protein)
siControl
siTRPC1
siTRPC3
siTRPC4
siTRPC6
F
PAH-hPASMCs
DMSO
MCV1
PDTC
100 kDa
TRPC3
43 kDa
β-Actin
TRPC3 protein relative expression
G
110 kDa
TRPC6
43 kDa
β-Actin
TRPC6 protein relative expression

Figure 2

Figure 2: TRPC channels are associated with exacerbated store-operated Ca^{2+} entry (SOCE) in pulmonary arterial hypertension (PAH)-human pulmonary arterial smooth muscle cells (hPASMCs). (A) Immunoblot and quantification of TRPC1 (n=6 patients), TRPC3 (n=4 patients), TRPC4 (n=11 patients), or TRPC6 (n=6 patients) in PAH-hPASMCs. (B) PAH-hPASMCs were transfected with siRNA against TRPC1 or TRPC3 or TRPC4, or TRPC6, and knockdown efficiency was assessed by RT-qPCR (n = 6 for each condition). (C) Consequence of TRPC1 or TRPC3 or TRPC4, or TRPC6 knockdown on their counterpart protein expression (n = 4-6 for each condition). (D) Consequence of TRPC1, TRPC3, TRPC4, or TRPC6 knockdown on SOCE amplitude in control-hPASMCs (n=9 patients with 173 cells for siControl, n=9 patients with 134 cells for siTRPC1, n=4 patients with 85 cells for siTRPC3, n=6 patients with 137 cells for siTRPC4, n=4 patients with 69 cells for siTRPC6). (E) Consequence of TRPC1, TRPC3, TRPC4 or TRPC6 knockdown on SOCE amplitude in PAH-hPASMCs. (n=8 patients with 196 cells for siControl, n=4 patients with 72 cells for siTRPC1, n=4 patients with 79 cells for siTRPC3, n=6 patients with 96 cells for siTRPC4, n=8 patients with 153 cells for siTRPC6). (F) Consequence of TRPC1, TRPC3, TRPC4 or TRPC6 knockdown on calcineurin activity in PAH-hPASMCs (n=6 patients for siControl, n=4 for siTRPC1 and TRPC4, n=5 for siTRPC3 and TRPC6). (G) Immunoblot and quantification of TRPC3 in PAH-PASMCs treated 48h with NFAT inhibitor (MCV1, 1 µmol/L) and NFκB inhibitor (PDTC, 1 µmol/L) (n=4 for DMSO and MCV1 and n=3 for PDTC). (H) Immunoblot and quantification of TRPC6 in PAH-PASMCs treated 48 h with NFAT inhibitor (MCV1 1 µmol/L) and NFκB inhibitor (PDTC, 1 µmol/L) (n=6 for DMSO and PDTC and n=5 for MCV1). Experiments presented in panels A-C were analysed using an unpaired t-test or Mann-Whitney test, and experiments presented in panels D-H- were analysed using the Kurskal-Wallis test. ns = non-significant; *P< 0.05, **P< 0.01, ***P<0.001, ****P<0.0001.

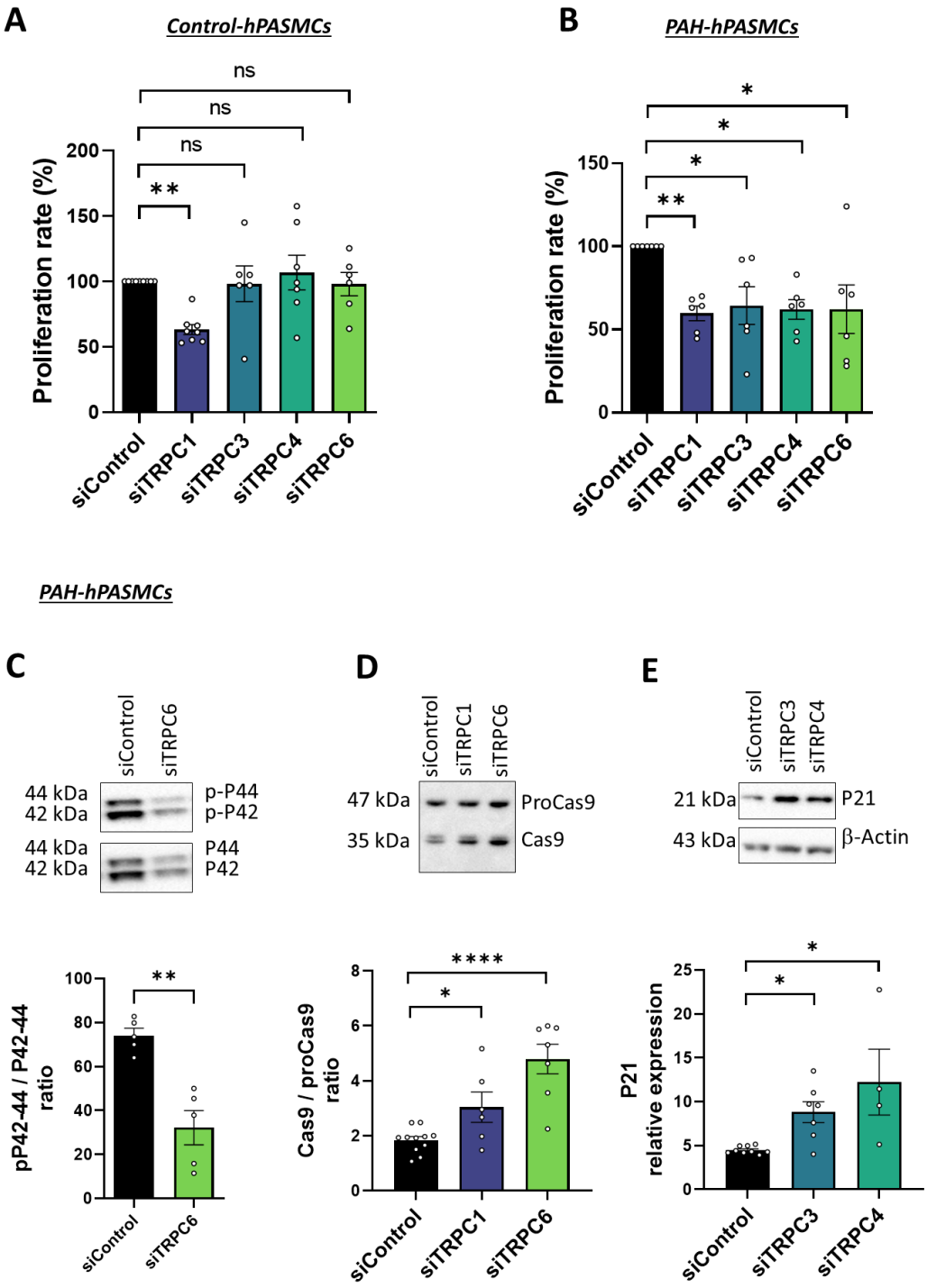

Figure 3

Figure 3: TRPC channels are associated with increased proliferation of PAH-hPASMCs. (A) Consequence of TRPC1, TRPC3, TRPC4, or TRPC6 knockdown on the proliferation rate (BrdU assay) of control-hPASMCs (n=9 patient for siControl, n=8 for siTRPC1, n=6 for siTRPC3 and siTRPC6 and n=7 for siTRPC4). (B) Consequence of TRPC1, TRPC3, TRPC4, or TRPC6 knockdown on the proliferation rate (BrdU assay) of PAH-hPASMCs (n=7 patient for siControl, n=6 for siTRPC1,

siTRPC3, siTRPC4, and siTRPC6). (C) Immunoblot and quantification of the consequence of TRPC6 knockdown on the pP42-44 / P42-44 ratio (n=5 patients). (D) Immunoblot and quantification of the consequence of TRPC1 or TRPC6 knockdown on the Caspase9 / proCaspase9 ratio (n=11 patients for siControl, n=6 for siTRPC1, and n=7 for siTRPC6). (E) Immunoblot and quantification of the consequence of TRPC3 or TRPC4 knockdown on P21 expression in PAH-PASMCs (n=9 patients for siControl, n=7 for siTRPC3, and n=4 for siTRPC4). Experiments presented in panels A-B, D-E were analysed with Kruskal–Wallis test, and panel C were analysed using the Mann-Whitney test. ns = non-significant; *P< 0.05, **P< 0.01, ****P< 0.0001.

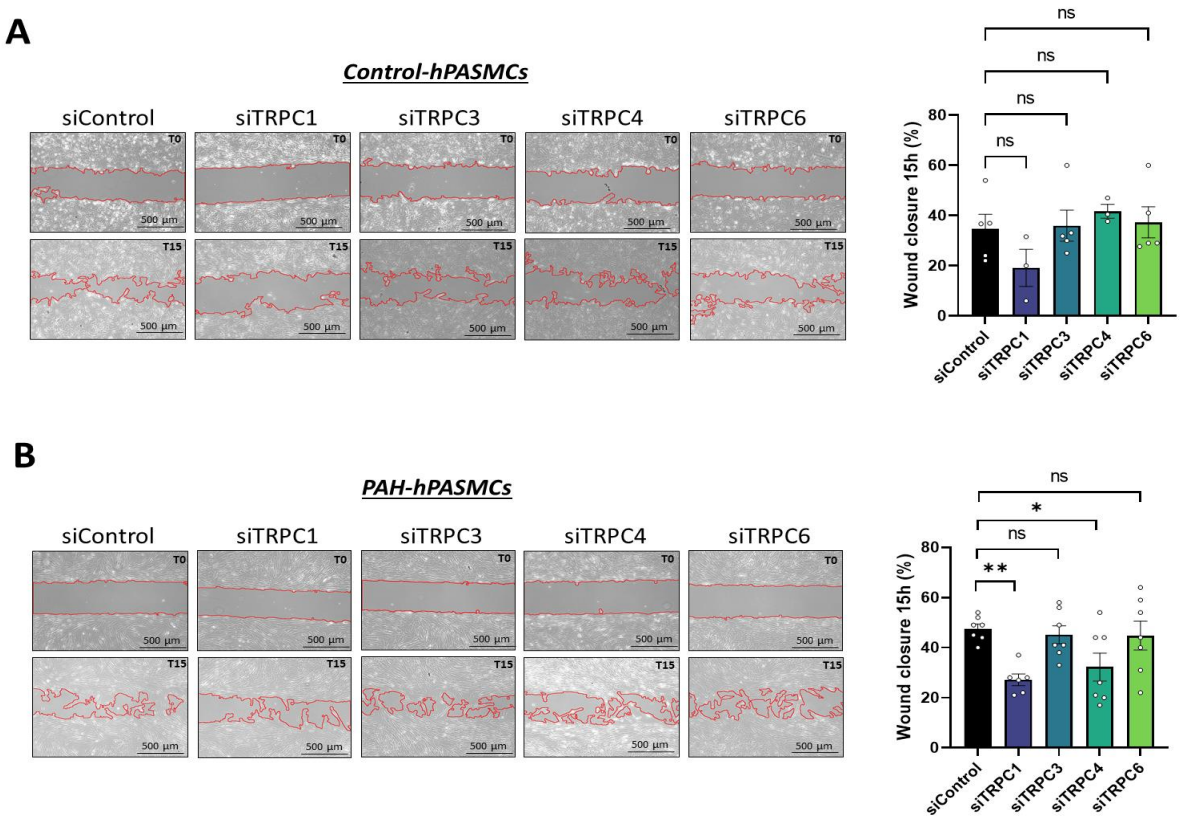

Figure 4

Figure 4: TRPC1 and TRPC3 channels contribute to the exacerbated migration of PAH-hPASMCs. (A) Wound-closure images (15 h after initiation) and percentage wound closure of the consequence of TRPC1, TRPC3, TRPC4, or TRPC6 knockdown in control-hPASMCs (n=5 patient for siControl, siTRPC3, and siTRPC6, n=3 for siTRPC1 and siTRPC4). (B) Wound-closure images (15 h after initiation) and percentage wound closure of the consequence of TRPC1, TRPC3, TRPC4, or

TRPC6 knockdown in PAH-hPASMCs (n=7 patient for siControl, siTRPC3, siTRPC4 and siTRPC6, n=6 for siTRPC1). Experiments presented in panel A-B with Kruskal–Wallis test. ns = non-significant; **P*< 0.05, ***P*< 0.01.

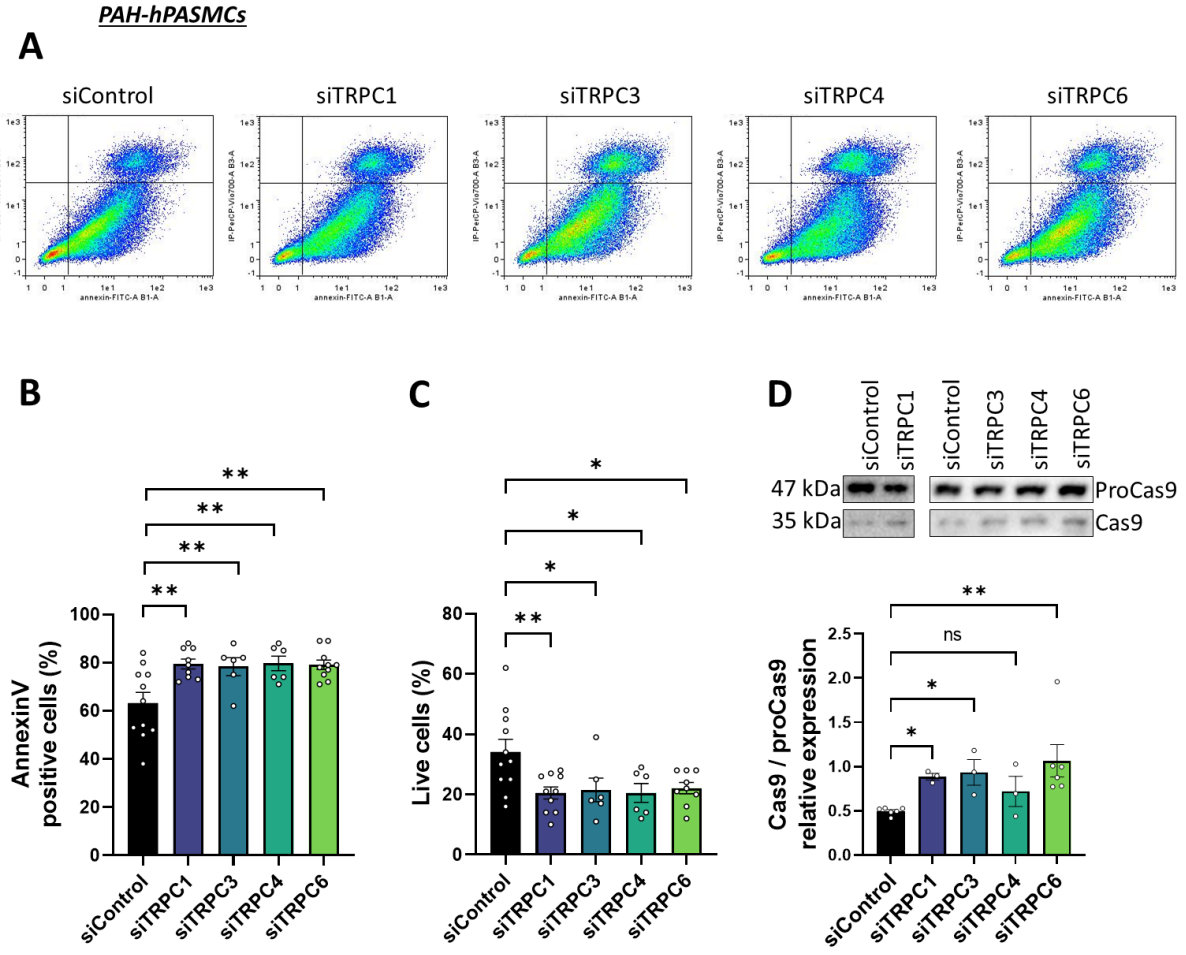

Figure 5

Figure 5: Knockdown of TRPC channels enhances apoptosis of PAH-hPASMCs exposed to staurosporine. (A) Dot plots of Annexin V+Propodium Iodide dual-labeling in PAH-PASMCs transfected with siControl, siTRPC1, TRPC3, TRPC4, or TRPC6 and exposed to 50 nmol/L staurosporine overnight. (B-C) Consequence of TRPC1, TRPC3, TRPC4, or TRPC6 knockdown on the percentage of Annexin V-positive and live PAH-hPASMCs exposed to 50 nmol/L staurosporine overnight (n=11 patient for siControl, n=9 for siTRPC1, n=6 for siTRPC3 and siTRPC4, n=10 for siTRPC6). (D) Immunoblots and quantification of the consequence of TRPC1, TRPC3, TRPC4, or TRPC6 knockdown on Caspase 9/proCaspase 9 ratio in PAH-PASMCs exposed to 50 nmol/L

staurosporine overnight (n=6 patient for siControl and siTRPC6, n=3 for siTRPC1, siTRPC3, and siTRPC4). Experiments presented in panels B-D were analysed with Kruskal–Wallis test. ns = non-significant; *P< 0.05, **P< 0.01.

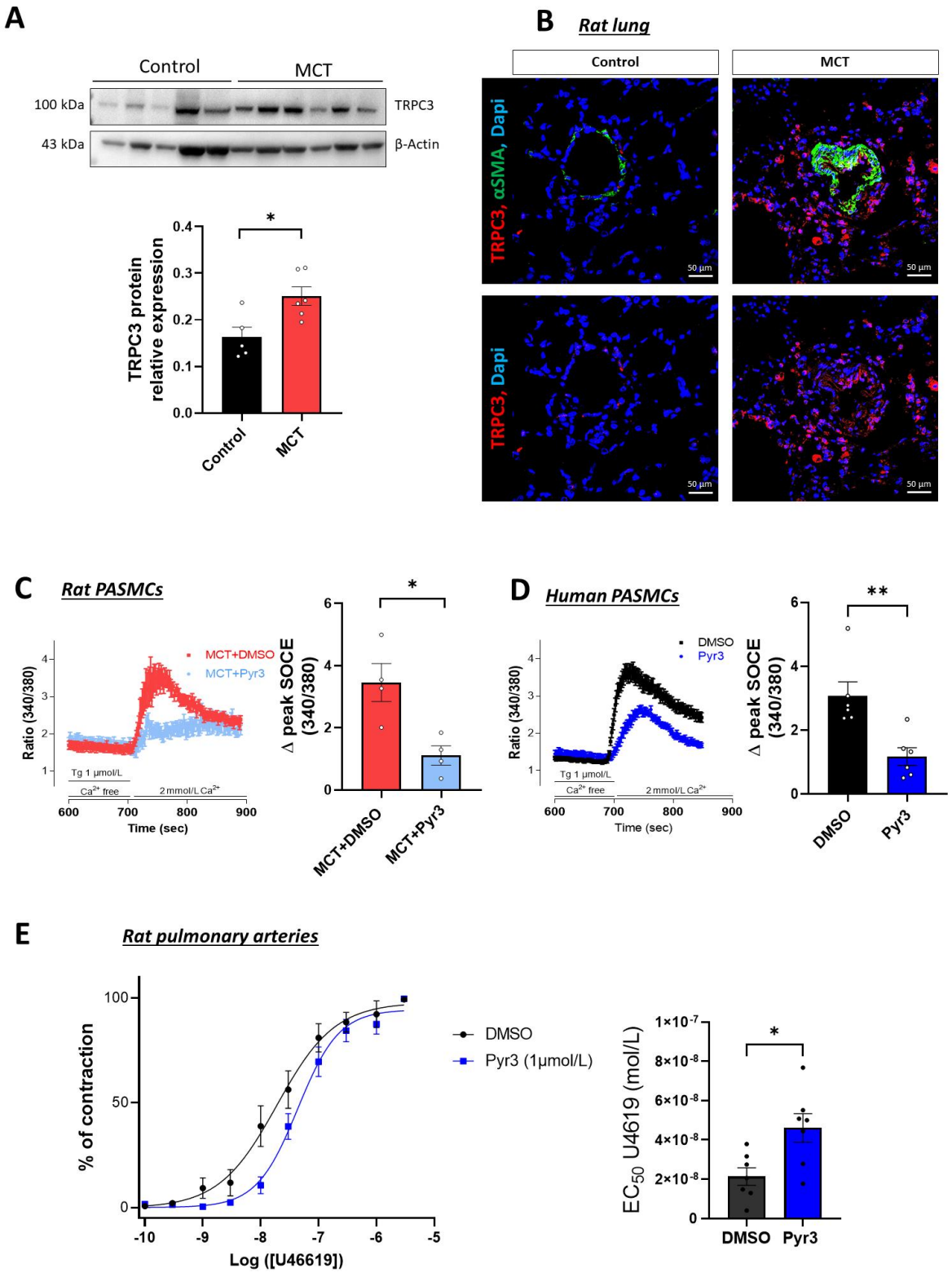

Figure 6

Figure 6: TRPC3 expression is increased in experimental pulmonary hypertension (PH)-induced by monocrotaline (MCT)-exposure in rats, and TRPC3 pharmacological blockade reduced SOCE in MCT-PASMCs. (A) Immunoblot and quantification of TRPC3 expression in lung tissue from control and MCT rats (n=5 for control rats and n=6 for MCT rats). (B) Localization and expression of TRPC3 immunofluorescence staining of paraffin-embedded lung sections from control- and MCT-rats at three weeks (Dapi staining (blue), TRPC3 staining (red) and αSMA staining (green)). Bar graph=50 µm. (C) SOCE and SOCE amplitude in MCT-rat PASMCs from rats treated with DMSO or Pyr3 (1 µmol/L, TRPC3 inhibitor) (n=4 rats with 45 cells for DMSO and n=4 with 46 cells for Pyr3). (D) SOCE and SOCE amplitude in PAH-hPASMCs treated with DMSO or Pyr3 (1 µmol/L) (n=6 rats with 67 cells for DMSO and Pyr3). (E, left panel) Dose-response curve (normalized to K100) was established by applying increasing concentrations of U46619 (a thromboxane A2 mimetic) on isolated rat pulmonary arteries in the presence of DMSO or Pyr3 (1 µmol/L). (E, right panel) Corresponding quantification of EC_{50} values (n=4 rats). Experiments presented in panels A-E were analysed using the Mann-Whitney test. ns= non-significant, *$P< 0.05$, **$P<0.01$.

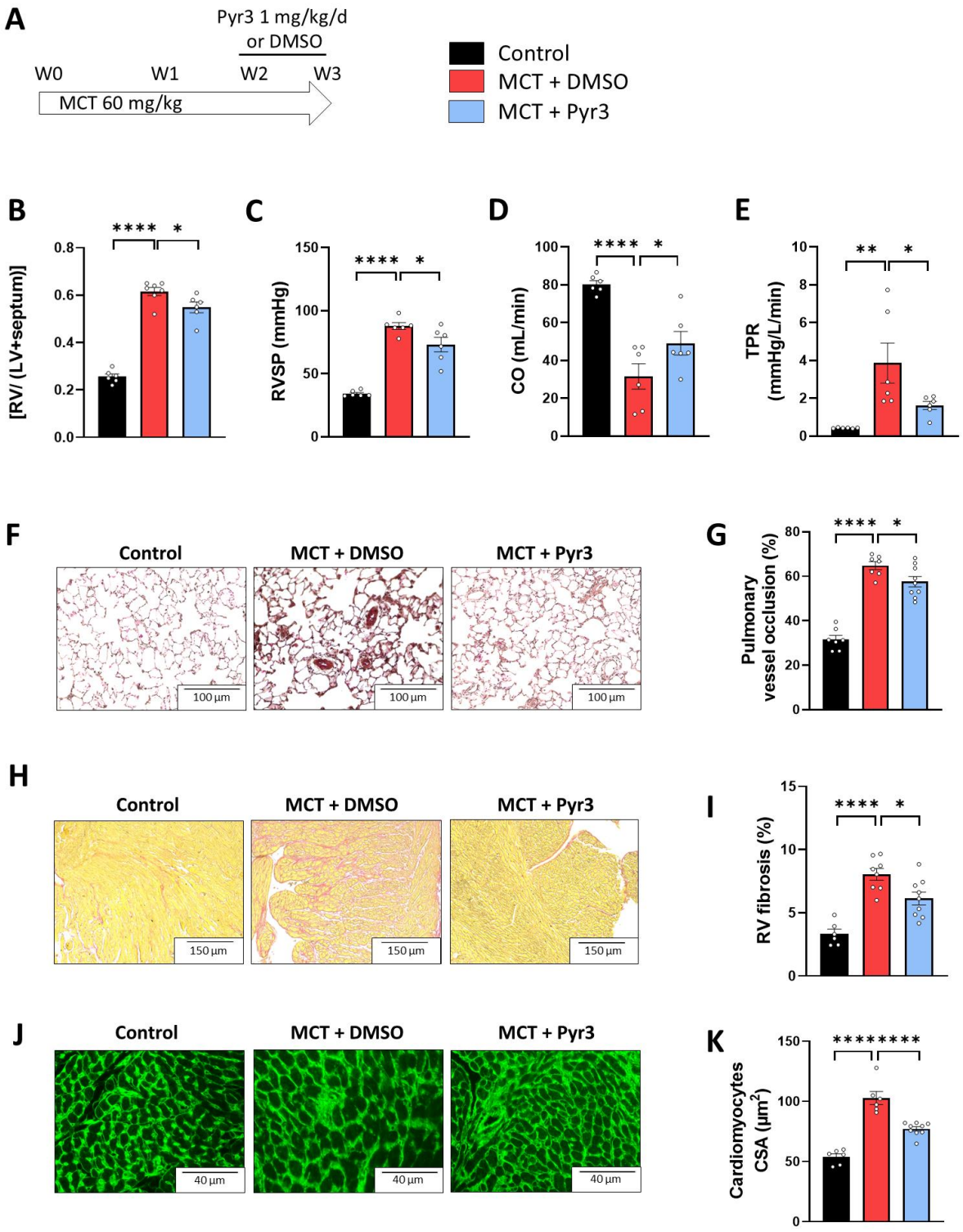

Figure 7

Figure 7: *In vivo* pharmacological inhibition of TRPC3 reduces the development of MCT-induced PH at pulmonary and right ventricular (RV) levels. (A) In *vivo* experimental design. Rats were injected subcutaneously with MCT at week 0 (W0) (60 mg/kg). DMSO or Pyr3 (1 mg/kg/day) was administered 7 days from week 2 (W2) to week 3 (W3) by intraperitoneal injection. (B) Fulton's index

(RV ÷ LV + septum) (n=6 rats for Control and MCT + Pyr3 group, n=7 rats for MCT + DMSO group). (C) Right ventricular systolic pressure (RVSP) in mmHg (n=6 rats). (D) Cardiac output (CO) in mL/min for Control (n=6 rats), MCT + Pyr3 (n=7 rats), and MCT + DMSO (n=7 rats) group. (E) Total pulmonary resistance (TPR) in mmHg/L/min (RVSP/CO) (n=6 rats). (F) Representative hematoxylin/eosin/Safran staining of paraffin-embedded lung sections from the control, MCT + DMSO, and MCT + Pyr3 groups. Scale bar, 100 µm. (G) Pulmonary vessel occlusion (%) in control (n=7 rats), MCT + DMSO (n=9 rats), and MCT + Pyr3 (n=9 rats) groups. (H) Representative interstitial fibrosis identified with Sirius red staining in RV compartment from control, MCT + DMSO, and MCT + Pyr3 groups. Scale bar, 200 µm. (I) Quantification of the percentage of fibrosis in RV tissue from control (n=6 rats), MCT + DMSO (n=8 rats), and MCT + Pyr3 (n=9 rats) groups. (J) Representative immunofluorescence images of RV sections stained with fluorescein isothiocyanate (FITC)–conjugated wheat germ agglutinin (WGA, 50 µg/mL, green) from the control, MCT + DMSO, and MCT + Pyr3 groups. Scale bar, 40 µm. (K) Quantification of cardiomyocytes cross-section area (CSA, n=30 cardiomyocytes measurement per rat for the control (n=6 rats), MCT + DMSO (n=6 rats), and MCT + Pyr3 (n=9 rats)). Experiments presented in panels B-E and G, I, and K were analysed using a one-way Anova test. *P< 0.05, **P< 0.01, ****P< 0.0001.